Assessment of Upscaling Methodologies for Daily Crop Transpiration using Sap-Flows and Two-Source Energy Balance Models in Almonds under Different Water Status and Production Systems

Manuel Quintanilla-Albornoz[1], Xavier Miarnau[2], Ana Pelechá[1], Héctor Nieto[3] and Joaquim Bellvert[1]

[1]Efficient Use of Water in Agriculture Program, Institute of Agrifood Research and Technology, Fruitcentre, Parc AgroBiotech, Lleida, 25003, Spain.
[2]Fruit Production Program, Institute of Agrifood Research and Technology, Fruitcentre, Parc AgroBiotech, Lleida, 25003, Spain.
[3] Institute of Agricultural Sciences, ICA-CSIC, Madrid, 28006, Spain.

Correspondence to: Manuel Quintanilla-Albornoz (manuel.quintanilla@irta.cat)

Abstract. Daily transpiration (T_d) is crucial for both irrigation water management and increasing crop water productivity. The use of the remote sensing-based two-source energy balance model (TSEB) has proven to be robust in estimating plant transpiration and evaporation separately for various crops. However, remote sensing models provide instantaneous estimations, so daily upscaling approaches are needed to estimate daily fluxes. Daily upscaling methodologies have not yet been examined to upscale solely transpiration in woody crops. In this regard, this study aims to evaluate the proper image acquisition time throughout the day and four methodologies to retrieve T_d in almond trees with different production systems and water status. Hourly transpiration (T_h) was estimated using the TSEB contextual approach (T_h-TSEB) with high-resolution imagery five times during two diurnal courses. The tested methodologies were the following: the simulated evaporative fraction variable (EF_{sim}), irradiance (*Rs*), reference evapotranspiration (ETo) and potential evapotranspiration (ETp). These approaches were first evaluated with in situ sap flow (T-SF) data and then applied to the T_h-TSEB. Daily T-SF showed significant differences among production systems and levels of water stress. The EF_{sim} and ETp methods correlated better with measured T-SF, and reduced the underestimation observed using the *Rs* and ETo methods, especially at noon in the severely water stressed trees. However, the daily upscaling approaches applied in the TSEB (T_d-TSEB) failed to detect differences between production systems. The lack of sensibility of T_h-TSEB among production systems poses a challenge when estimating T_d in canopies with discontinuous architectural structures. The use of ETp as a reference variable could address this issue, as it incorporates various aerodynamic and radiative properties associated with different canopy architectures that influence the daily T_h-SF pattern. However, more accurate ETp estimates or more advanced ETp models are needed.

1 Introduction

Almond is one of the high-value crops with the greatest water usage (Goldhamer and Fereres, 2017; López-López et al., 2018). In Spain, a paradigm change is taking place with the introduction of new intensified almond production systems with more

planar designs (Iglesias and Echeverria 2022), which may complicate the accurate estimation of evapotranspiration (ET) using remote sensing models. Thus, since the expansion of almond production is occurring in a context of increasing water scarcity, many studies have focused on quantifying its water usage in different environments and water regimes. From a water management point of view, there is particular interest in validating the daily ET and its components, transpiration (T) and evaporation (E), in this crop and under different production systems and water status. This is relevant because almond is considered a drought-tolerant species able to control water loss through stomatal closure, which has been identified as a common and early event in plant response to water deficit (Castel and Fereres, 1981, Escalona et al. 1999, Chaves et al. 2002). Romero et al. (2006) also showed that the influence of the evaporative demand of the atmosphere on stomatal behaviour was higher under well-watered compared to water-stressed almonds. The same study also demonstrated that water-stressed almonds restricted stomatal activity earlier in the morning when atmospheric vapor pressure deficit (VPD) was still low. As a result, maximum T values occurred during this period and were significantly higher than those observed in well-watered almonds.

Accurate in-field quantification of crop ET and the partition components E from soil and plant T is very useful for both irrigation water management and increasing crop water productivity (Zhang et al. 2021). Consequently, several methodologies have been developed to address this objective (Evett and Tolk 2009). Of these, remote sensing thermal-based surface energy balance models have shown their utility in retrieving ET in a wide range of environments and ecosystems (Shuttleworth and Wallace 1985; Bastiaanssen et al. 1998; Drexler et al. 2004; Overgaard et al. 2006; Allen et al. 2007; Timmermans et al. 2007; Kalma et al. 2008; Kustas and Anderson 2009). The advantage of using remote sensing lies in the possibility of monitoring heterogeneous surfaces over a wide range of spatial resolutions and thereby generating operational ET products (Kalma et al. 2008). One such model that calculates T and E explicitly is the two-source energy balance (TSEB), which was initially developed by Norman et al. (1995) and Kustas and Norman (1999). The separate T and E outputs provide the advantage of simultaneously evaluating canopy stress and directly quantifying plant water consumption. This information can be valuable for enhancing water use efficiency in agricultural and environmental management. Moreover, T is also linked to plant productivity as the exchange of both water and carbon between the atmosphere and the plant is conveyed via the leaf stoma. The TSEB approach has demonstrated its robustness in accurately estimating plant ET across diverse surface conditions and a wide range of landscapes (Kustas and Anderson 2009; Kustas et al. 2019; Gómez-Candón et al. 2021; Gao et al. 2023; Knipper et al. 2023). To estimate T, the use of very high resolution thermal and multispectral imagery allows for the direct estimation of canopy (T_c) and soil temperature (T_s), facilitating the retrieval of ET partitioning, through use, for example, of the TSEB contextual approach (TSEB-2T) model (Nieto et al. 2019; Nassar et al. 2020; Gao et al. 2023; Quintanilla-Albornoz et al. 2023).

Models for estimating ET fluxes based on remote sensing, however, can only be used to derive an instantaneous ET at the time of clear-sky satellite or aircraft overpass. Thus, the selection of a proper overpass time and the development of upscaling algorithms to extrapolate ET from instantaneous to daily scale are of special interest for the management of crop water consumption. Current thermal infrared (TIR) polar orbiting satellites, such as Landsat, Sentinel-3 or the moderate-resolution imaging spectroradiometer (MODIS) on board Terra, have an overpass time close to 10:00 am (mean locator solar time).

However, several studies suggest that the best accuracies in ET retrievals would be captured better in the early afternoon (Delogu et al. 2012; Anderson et al. 2021). Bellvert et al. (2014) also showed that early afternoon was the most appropriate moment to detect maximum differences in T_c between well-watered and water-stressed crops. For this reason, in coming years new TIR satellite missions including TRISHNA (Thermal infraRed Imaging Satellite for High Resolution Natural resource Assessment) (Lagouarde et al. 2018), SBG (Surface Biology and Geology) (Basilio et al. 2022), or LSTM (Land Surface Temperature Monitoring) (Koetz et al. 2018) are planned at an overpass time around 13:00 hours (GMT time).

Daily upscaling of ET fluxes is commonly performed by assuming a constant relationship over the course of the day between instantaneous ET and a reference meteorological forcing that can be computed at hourly and daily timesteps (Crago and Brutsaert 1996; Van Niel et al. 2011; Cammalleri et al. 2014). This hypothesis is generally known as self-preservation (Crago and Brutsaert 1996). Generally, the most commonly used methods for upscaling ET are: the evaporative fraction (EF) method, the solar radiation (*Rs*) method, the stress factor method and the canopy resistance method (Hoedjes et al. 2008; Delogu et al. 2012; Cammalleri et al. 2014; Jiang et al. 2021; Nassar et al. 2021). Experimental studies have shown that the EF method, which is based on the ratio between latent heat flux (*LE*) and the available energy at the surface (AE), is relatively stable during midday hours for days with clear sky conditions, but significantly higher during early morning and late afternoon. These differences in EF during the day cause a systematic underestimation of daytime average values under wet conditions (Shuttleworth et al. 1989; Brutsaert 1992; Crago and Brutsaert 1996; Lhomme and Elguero 1999; Gentine et al. 2007). To address this challenge, Hoedjes et al. (2008) introduced a parameterization of the diurnal EF pattern based on the primary atmospheric forcing parameters: *Rs* and relative humidity (RH). Implementing this approach, known as EF_{sim}, Delogu et al. (2012) successfully reduced the overestimation associated with the EF method from 15.8% to 6.5%.

Additionally, while estimating the instantaneous AE at a specific time can be relatively straightforward using thermal imagery and meteorological data, determining daily AE needs daily course measurements or estimates of net radiation (R_n) and soil heat flux (G), which can be challenging. Given that the diurnal pattern of AE is primarily influenced by *Rs*, it has become a common practice to use *Rs* as a reference variable for the estimation of daily ET fluxes from instantaneous measurements (Jackson et al. 1983; Zhang and Lemeur 1995). The use of *Rs* in the context of remote sensing applications has fewer requirements than the EF method, with the latter needing auxiliary information such as R_n that can be complex to measure and may further limit operational utility. When used the *Rs* upscaling method, both Cammalleri (2014) and Nassar (2021) improved daily ET compared to EF methods.

Another upscaling method that has been proposed is the stress factor method. This approach employs the reference evapotranspiration (ETo) or potential evapotranspiration (ETp) as a reference variable, which inherently accounts for the key meteorological factors influencing the evaporative process (Trezza 2002; Delogu et al. 2012). Trezza (2002) found a constant ratio between ET and ETo during the daytime and employed it to estimate daily ET using remote sensing estimations, achieving better results compared to EF upscaling methods. However, Cammalleri (2014) obtained similar results when using both the EF method and the ETo to estimate daily ET in sites without stress conditions. For their part, Delogu et al. (2012) evaluated the use of ETp as a reference variable and obtained worse results compared to the EF method for a dataset with stress events.

This was attributed to the fact that the AE followed both stressed and unstressed ET patterns, whereas ETp often increased independently of the water stress levels.

Nevertheless, the aforementioned upscaling methods reported in the literature in agricultural ecosystems have only been validated against daily ET, usually over sites with eddy-covariance flux towers, with a footprint with mixed information on the spatial variability (Cammalleri et al. 2014, Xu et al. 2018, Jiang et al. 2021). Therefore, to the best of our knowledge, the use of upscaling methodologies to estimate daily T (T_d) based on instantaneous T values has not been previously examined. Furthermore, the diurnal pattern of T has a different response between well-watered and water-stressed crops (Poni et al. 2009, Tuzet et al. 2003), and this different response would also depend on the stomatal control of each species to soil water and vapor pressure deficits. Thus, the hypothesis of this study is that upscaling methods may have different responses for water-stressed and well-watered almond trees (Sánchez et al. 2021; Jofre-Čekalović et al. 2022; Iglesias and Echeverria 2022; Peddinti and Kisekka 2022; Knipper et al. 2023). Therefore, the main purpose of this study is to evaluate different T_d upscaling methodologies in almond trees under different production systems and water regimes using sap flow measurements. This study aims to contribute to our understanding and establish a reference for upscaling remote sensing canopy T in woody crops, which is crucial in mapping daily ET partitioning from field to global scales.

2 Materials and Methods

2.1 Trial location and design

This study was conducted in an almond orchard situated at the experimental station of the IRTA (Institute of Agrifood Research and Technology) in Les Borges Blanques, Spain (41°30'31.89''N; 0°51'10.70''E, 323 m elevation) (Fig. 1a). The almond orchard was planted in June 2009, with "Marinada" used as the scion cultivar onto an INRA GF-677 rootstock. Additionally, the orchard was planted with different planting distances and subjected to different pruning techniques. The combination of planting distance and pruning techniques will be referred to as "production system". Three almond production systems were evaluated: open vase with minimal pruning (MP) spaced at 5.5 x 3.5 m, central axis at 5 x 3 m, and hedgerow at 4.5 x 3 m (Fig. 1b and Fig. 1c). The orchard was situated on a clay loam-textured soil, with a depth ranging from 1.6 to 2 m. The study site has a Mediterranean climate, with an average annual rainfall of 364 mm and an average annual evapotranspiration of 1088 mm. Two different dates were selected to assess the diurnal course of T: 29th June and 19th August 2022. Figure 2 displayed the meteorological conditions during the campaign.

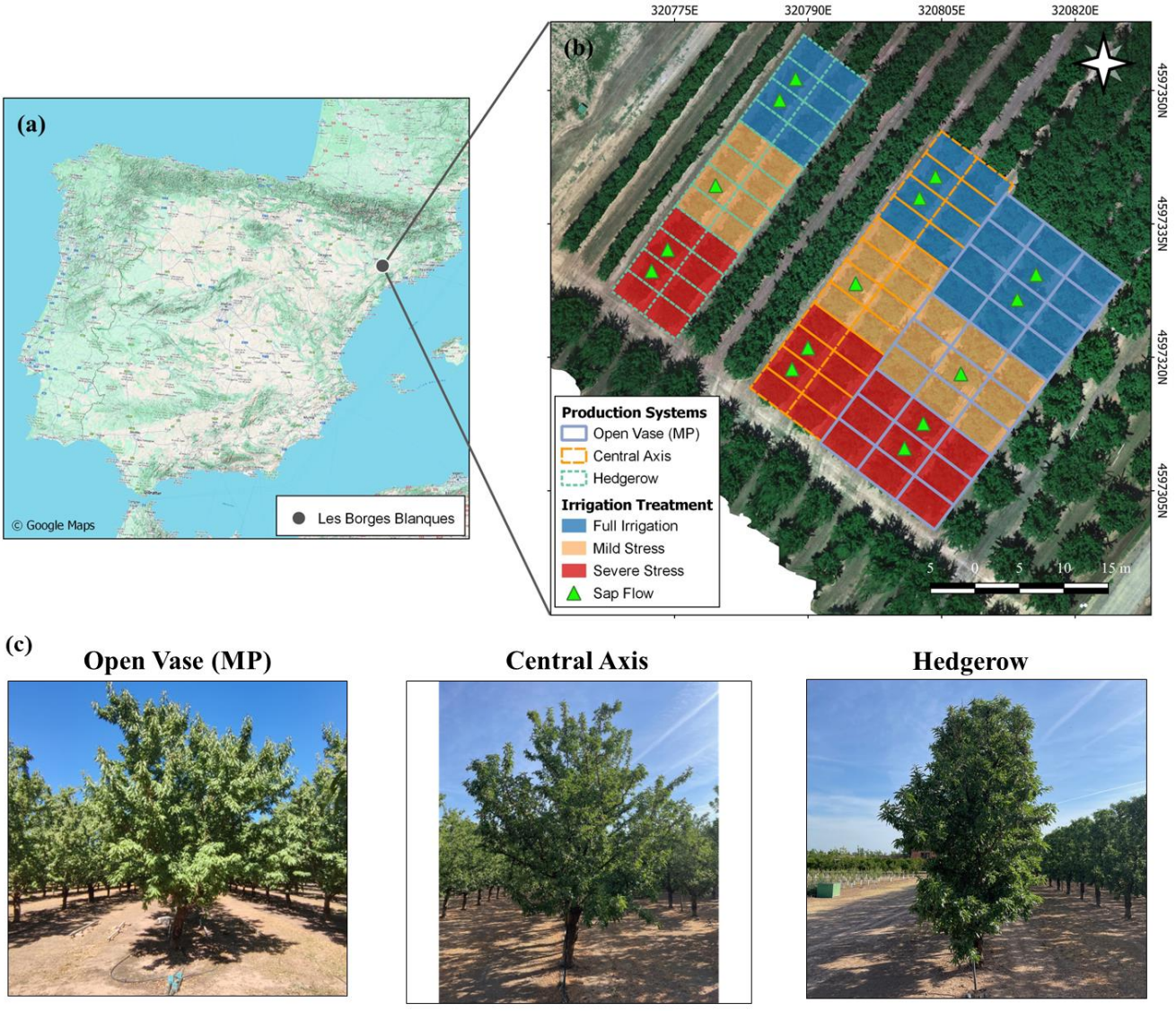

Figure 1: (a) Location of the almond orchard in Les Borges Blanques, (b) experimental design of the orchard, showing in different colours the three production systems and the three irrigation treatments and (c) photographs from summer 2022 of production systems.

130

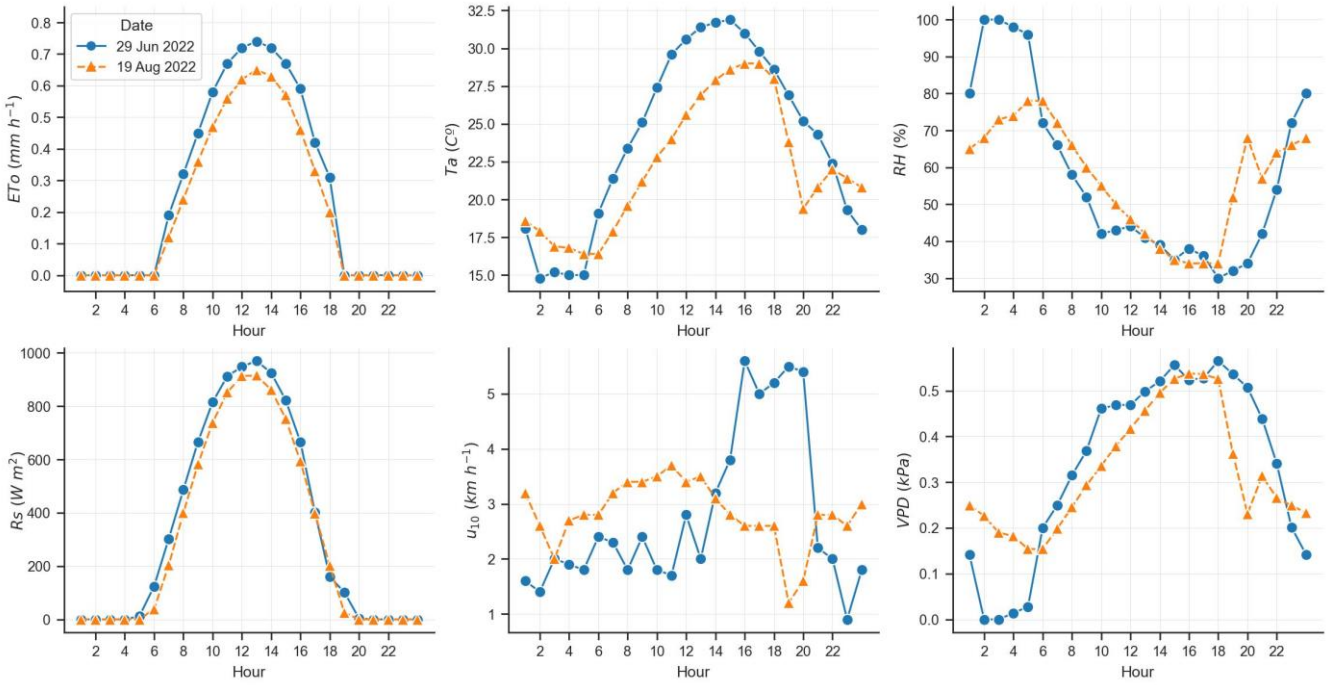

Figure 2. Meteorological conditions at hour scale during the flight campaign.

The orchard was irrigated using a drip irrigation system. In the open vase (MP) system, two lateral pipes were positioned on each side of the tree at 40 cm, with a dripper placed every 70 cm and a water discharge rate of 2.2 l h^{-1}. The central axis and hedgerow systems had a lateral pipe along the row line, with drippers placed at 60 cm intervals with a water discharge rate of 3.8 l h^{-1} per dripper. Daily irrigation was scheduled on a weekly basis to complement potential crop evapotranspiration (ETc) using: ETc = (ETo x Kc) – effective rainfall, as described by Allen et al. (1998). ETo was obtained from a meteorological station within Catalonia's official network of meteorological stations (SMC, https://ruralcat.gencat.cat/web/guest/agrometeo), situated 500 m away from the study site. The ETo is estimated using the FAO56 Penman-Monteith method (Allen et al. 1998). Kc refers to the crop coefficient. The Kc was assigned based on different phenological stages, following Goldhamer and Girona (2012). The assigned Kc values were: Kc_1 = 0.70 (April), Kc_2 = 0.95 (May), Kc_3 =1.09 (June), Kc_4 = 1.15 (July), Kc_5 = 1.17 (August), and Kc_6 = 1.12 (September). Effective rainfall was determined following the method outlined by Olivo et al. (2009), which considers half of the precipitation for days with a single event exceeding 10 mm, otherwise, it is considered zero. Three irrigation treatments were implemented for each production system during the 2021 and 2022 growing season: (i) Full irrigation, where irrigation matches ET requirements (100% ETc); (ii) mild stress, irrigated at 50% ETc; and (iii) severe stress, irrigated at 20% ETc. The water applied was quantified using digital water meters (CZ2000-3M, Contazara, Zaragoza, Spain).

2.2 Sap flow measurement

Sap flow sensors offer substantial advantages, enabling the continuous and automated measurement of sap movement for each plant with a high temporal resolution (Smith and Allen 1996; Forster 2017; Fernandez 2001). When properly calibrated, these sensors can measure the T for the entire plant (López-Bernal et al. 2010; Forster 2017; Noun et al. 2022). Among the sap flow measuring methods available, the compensation heat pulse (CHP) has been suggested as a tool for detecting water stress and for irrigation scheduling purposes (Fernandez 2001; Alarcón et al. 2005). Therefore, the CHP sap flow method combined with the calibrated average gradient technique was employed to estimate the T. The sap flow system consists of a 2 mm diameter 4.8 W stainless steel heater and two temperature sensors positioned 10 and 5 mm downstream and upstream of the heater, respectively. Each temperature sensor is embedded with two E-type thermocouples (chrome-constantan wire) spaced 10 mm apart along the needle. The heat pulse velocity at 5 and 15 mm below the cambium is used to calculate the sap flow density across the trunk radius. The sap flow system was developed by the IAS-CSIC laboratory. For further specifications, refer to Villalobos et al. (2009). Sap flow data were collected every 15 minutes and stored in a CR1000 datalogger (Campbell Scientifc Inc., Logan, UT, USA).

Sap flow sensors were installed in each production system, monitoring two trees from the full irrigation and severe stress treatments, and one tree from the mild stress treatments, as shown in Figure 1b. They were installed at 0.5 m above the ground. Each sap flow transpiration (T-SF) underwent correction for wound and azimuthal effects (López-Bernal et al. 2010) using actual T measured by a water balance method (T_{wb}) on July 13, 2022. The T_{wb} was calculated using Eq. (1).

$$T_{wb} = P + I_R - \Delta SWC - DP - E, \quad (1)$$

Where P is precipitation, I_R is the amount of water applied through irrigation, ΔSWC is the difference in soil water content (SWC) between two consecutive days, DP is deep percolation and E corresponds to evaporation. P, DP and I_R were considered zero because the water balance was calculated for days without P and I_R applied. Additionally, the soil was covered with plastic sheeting during these days to prevent E fluxes ($E \approx 0$). Differences between T_{wb} and T-SF measurements were assumed to remain constant throughout the season, as demonstrated by Espadafor et al. (2015). The calibrated T-SF was used to calculate both the accumulated hourly T (T_h-SF) and the accumulated daily T (T_d-SF).

The SWC was measured using a neutron probe at intervals of 20 cm down to a depth of 180 cm (Campbell Pacific Nuclear Scientific, Model 503). The tubes used for SWC measurements were installed to cover one quarter of the planting area. In each tree, two groups of three tubes were installed in parallel, positioned below the emitter, at a quarter of the inter-row distance, and at half of the inter-row distance. Soil sampled were taken at the time of tubes installation to estimate the volumetric moisture content (cm^3 of water cm^{-3} of soil). This measurement was then used to calibrate the neutron probe readings.

2.3 Field measurement

2.3.1 Stem water potential, stomatal conductance, leaf transpiration and leaf area index

Stem water potential (Ψ_s), stomatal conductance (g_s) and leaf transpiration (E_{leaf}) were measured at 7:00, 9:00, 12:00, 14:00 and 16:00 solar time during the UAV flight campaign and in the same trees where sap flow sensors were installed. The measurement of Ψ_s followed the protocol outlined by McCutchan and Shackel (1992). The Ψ_s was determined by measuring three shaded leaves from each tree. Prior measurement, each leaf was enclosed in a plastic bar covered with aluminium foil for one hour to equalize the water potential between the leaf, stem, and branches. A pressure chamber (Plant Water Status Console, Model 3500; Soil Moisture Equipment Corp., Santa Barbara, CA) was utilized to obtain the Ψ_s in all measurement within one hour. The g_s and E_{leaf} were measured using the LI-600 porometer/fluorometer (LI-COR Inc., Lincoln, NE, USA). Three sunny leaves were measured in each tree concomitant to image acquisition. The leaf area index (LAI) was determined for trees equipped with sap flow sensors using the LAI-2200 Plant Canopy Analyzer (PCA) (LI-COR Inc., Lincoln, NE, USA) The LAI was measured in each flight date around midday. The LAI measurement procedure involved one measurement taken above the tree and four below the tree. The incident radiation above the tree was recorded in an open area using five sensor rings. A single measurement was taken in each cardinal direction (N, S, E and W) beneath the tree. The LAI was subsequently estimated from the vertical profile of the crown using the FV2200 v. 2.1.1 software. The accuracy of LAI estimations was 0.57 m^2 m^{-2} (Quintanilla-Albornoz et al. 2023).

2.3.2 Image acquisition campaign

Ten flights were conducted on June 29 and August 29 of 2022 with UAV Dronehexa XL (DRONETOOLS, Seville, Spain). On each day, five flights were conducted at 7:00, 9:00, 12:00, 14:00 and 16:00 GMT. The UAV was outfitted with a Micasense RedEdge-MX multispectral camera (Micasense, Northlake Way, Seattle, USA) and a FLIR SC655 thermal camera (FLIR Systems, Wilsonville, OR, United States). Micasense RedEdge-MX captures images in five spectral bands at wavelengths of 475 ± 20 nm, 560 ± 20 nm, 668 ± 10 nm, 717 ± 10nm, and 840 ± 40 nm. FLIR SC655 has a spectral response in the range of 7.5–13 µm. The flights were carried out at a height of 50 m above ground level to capture multispectral and thermal images with spatial resolutions of 0.03 m and 0.06 m, respectively.

All images were subjected to radiometric, atmospheric and geometric correction. The FieldSpec 4 Standard-Res spectroradiometer (Malvern Panalytical, Inc., United Kingdom) was used to acquire in situ spectral measurements on various ground target simultaneously with the image acquisition for radiometric calibration. The FieldSpec 4 Standard-Res spectroradiometer has an optical resolution of 3-10 mm and a wavelength response between 350 and 2500 nm. Before conducting spectral measurements on the ground targets, the spectroradiometer was calibrated using white reference panel (white color SpectralonTM) and a dark reference. The thermal sensor underwent radiometric calibration in the laboratory using a blackbody (model P80P, Land Instruments, Dronfield, United Kingdom). Additionally, in-situ temperature measurements were acquired using an SI-111-SS Apogee infrared radiometer connected to an Apogee AT-100 microCache Bluetooth

micrologger (Apogee instruments Inc, Logan, UT, USA). The mosaicking process, as well as the generation of the digital elevation model (DEM) and the digital surface model (DSM), were performed using Agisoft Metashape Professional software (Agisoft LLC., St. Petersburg, Russia). Geometric and radiometric corrections was conducted using QGIS 3.4 (QGIS 3.4.15).

2.4 TSEB model description

The TSEB scheme, initially introduced by Norman et al. (1995) and further refined by Kustas and Anderson (2009), was utilized to estimate T employing high-resolution images. The TSEB is an energy balance models that assumes net surface radiation (R_n) is primarily distributed among sensible heat flux (H), latent heat flux (LE) and soil heat flux (G). Consequently, the LE (W m^{-2}) is calculated as the residual of the surface energy equation by Ep. (2.1), Eq. (2.2) and Eq. (2.3):

$$LE \approx R_n - H - G, \quad (2.1)$$

$$LE_s \approx R_{n,s} - H_s - G, \quad (2.2)$$

$$LE_c \approx R_{n,c} - H_s, \quad (2.3)$$

Where the subscripts $_C$ and $_S$ refer to the energy fluxes of the canopy and soil, respectively. The Campbell and Norman (1998) canopy transfer model, considering a rectangular clumping index, was employed to estimate $R_{n,s}$ and $R_{n,c}$, as described by Parry et al. (2019) and Quintanilla-Albornoz et al. (2023). G was assumed as a constant fraction of $R_{n,s}$ of around 0.35. A series resistance scheme was utilized, dividing H into soil (H_s) and canopy (H_c) as shown in Eq. (3.1), Eq. (3.2) and Eq. (3.3):

$$H_s = \rho C_p \frac{T_s - T_{ac}}{r_s}, \quad (3.1)$$

$$H_c = \rho C_p \frac{T_c - T_{ac}}{r_x}, \quad (3.2)$$

$$H_s + H_c = \rho C_p \frac{T_{ac} - T_a}{r_a}, \quad (3.3)$$

where ρ is the air density, C_p is the specific heat of air, T_s is the soil temperature, T_c is the canopy temperature, T_a is the air temperature, T_{ac} is the temperature in the canopy air space, equivalent to the aerodynamic temperature, r_s is the resistance to heat flow in the boundary layer immediately above the soil surface, r_x is the total boundary layer resistance of the complete canopy leaves, and r_a is the aerodynamic resistance to turbulent heat transport between the air canopy layer and the overlying air layer. The resistances were derived according to Kustas and Norman (1999) and Norman et al. (1995).

The contextual approach of the TSEB model (TSEB-2T) was evaluated in this study and is available online at https://zenodo.org/doi/10.5281/zenodo.594732. The TSEB-2T was applied with direct measurements of T_c and T_s from high-resolution thermal images. T_c and T_s were obtained with a supervised image classification based on using the DSM and the soil-adjusted vegetation index (SAVI). SAVI was chosen due to its ability to reduce the impact of ground brightness in the near and shortwave infrared wavelengths, which enhances the contrast between vegetation and the ground surface (Qi et al. 1994). Pixel were classified as canopy if they exhibited a DSM greater than 1.5 m and a SAVI greater than 0.2. Pixels that did

not meet these conditions were classified as pure soil. These layers were employed to retrieval the T_c and T_s from thermal images. Finally, the hourly T in mm (T_h-TSEB) was estimated using: $1000 \times 3600 \times LE_c$ / ($\rho_w \lambda$), where ρ_w is the density of water (assumed to be 1,000 kg m^{-3}) and λ is the latent heat of vaporization (J kg^{-1}): $\lambda = 1e^6 \times (2.501 - 0.002361\ T_a)$. All biophysical traits required for TSEB models, the fractional canopy cover (*fc*), canopy height (*hc*) and canopy width (*wc*), were obtained using the multispectral and DSM high resolution images. For additional details on the biophysical traits' procedure, refer to Quintanilla-Albornoz et al. 2023.

2.5 Models evaluated to upscale daily transpiration

The self-conservation method is the most commonly used approach to upscale ET fluxes from instantaneous measurements. This assumes a constant relationship between the instantaneous ET and some meteorological variables over time under certain conditions. According to Cammalleri (2014), the relationship between instantaneous measurement of ET fluxes and a reference variable can be illustrated using Eq. (4):

$$ET_d = \beta \frac{1}{\lambda} \frac{\lambda LE_t}{X_t} X_d, \quad (4)$$

where λLE_t is the instantaneous latent heat flux at the acquisition time *t*, X_t and X_d are the values of the reference variable at the acquisition time *t* and during the day *d*, and β represents a correction factor to account for potential biases or nighttime ET. This paper evaluates four self-preservation approaches, elucidated below, along with their implications for estimating T_d in almond crops.

2.5.1 Simulated evaporative fraction variable (EF_{sim}) method

The EF_{sim} is based on the evaporative fraction (EF) method. The EF method assumes that the ratio between *LE* and AE is relatively constant during the day. Following Eq. (5.1), Eq. (5.2) and Eq. (5.3), we can obtain the daily *LE* fluxes:

$$EF = \frac{LE}{\mathrm{AE}} \quad (5.1)$$

$$\mathrm{AE} = R_n - G \quad (5.2)$$

$$LE_d = \mathrm{AE_d} \times EF \quad (5.3)$$

where LE_d and AE_d correspond to daily accumulated *LE* and AE, respectively. R_n can be determined from remote sensing data using Eq. (6):

$$R_n = (1 - \alpha) \cdot R_S + \varepsilon \cdot R_{atm} - \varepsilon \cdot \sigma \cdot T_{rad} \quad (6)$$

where α corresponds to the albedo, ε the surface emissivity, R_{atm} the atmospheric longwave radiation, σ the Stefan-Boltzman constant, and T_{rad} the radiometric temperature. To avoid daily measurement of R_n and *G*, the AE can be extrapolated from instantaneous AE estimated through thermal imagery and *Rs*, following the methods proposed by Jackson et al. (1983) and Delogu et al. (2012), as expressed in Eq. 7:

$$AE_d = Rs_d \frac{AE_t}{Rs_t} \quad (7)$$

where AE_t represents the instantaneous AE estimated through thermal imagery, Rs_d the daily *Rs*, and Rs_t is the *Rs* at the measurement time. According to Hoedjes et al. (2008), the daily pattern of EF can be simulated as a function of *Rs* and RH, as in Eq. (8.1). However, EF_{sim} is a theoretical curve and must be adjusted using real EF values with Eq. (8.2):

$$EF_{sim} = 1.2 - \left(0.4 \frac{Rs}{1000} + 0.5 \frac{RH}{100}\right) \quad (8.1)$$

$$EF_{adj} = EF_{sim} \frac{EF_{t,obs}}{EF_{t,sim}} \quad (8.2)$$

where *Rs* is in W m^{-2} and RH is in percentage. Additionally, $EF_{t,obs}$ represents actual EF values estimated using remote sensing imagery based on Eq. (5.1), and $EF_{t,sim}$ is the EF_{sim} at the time of $EF_{t,obs}$. Finally, the EF_{sim} method employs Eq. (5.3) with an EF estimated using Eq. (8.2) and AE_d estimated using Eq. (7) to estimate LE_d.

2.5.2 Incoming shortwave solar radiation (*Rs*) approach

An alternative strategy consists of replacing AE as a reference variable with the *Rs*. This method is founded on the principle that *Rs* is the primary radiation flux during the day, resulting in a strong correlation and associated variations between actual ET and *Rs* (Jackson et al. 1983; Delogu et al. 2012, Nassar et al. 2021). Thus, LE_d can be estimated with Eq. (9):

$$LE_d = Rs_d \frac{LE_t}{Rs_t} \quad (9)$$

where Rs_d corresponds to daily *Rs* and Rs_t is the *Rs* at the time that *LE* was estimated.

2.5.2 Stress factor approach

The stress factor approach involves upscaling the instantaneous ET using either reference (ETo) or potential evapotranspiration (ETp), as depicted in Eq. (10):

$$ET_d = SF \cdot ET_O(ET_p) \quad (10)$$

The stress factor is defined as the ratio between ET and instantaneous ETo or ETp (*SF = ET/ETo (or ETp)*). The ETo was obtained using the FAO-56 method (Allen et al., 1998). ETp was estimated using the Penman Monteith one-source energy balance model, and forcing it with meteorological data and the actual LAI (Allen et al., 1998). The ETp obtained from the Penman Monteith model is available in the Python programming language at https://zenodo.org/doi/10.5281/zenodo.594732. The minimum bulk canopy resistance for the ETp model was determined through a method that parameterizes the relationship between g_s and VPD, as describe by Kustas et al., (2022). Meteorological data were obtained from the weather station of the Meteorological Service of Catalonia located near the experimental orchard.

The EF_{sim}, *Rs*, ETo and ETp upscaling methods were used to estimate T_d from T_h-SF measurements and from T_h-TSEB estimations. The T_d obtained using the EF_{sim}, *Rs*, ETo and ETp upscaling methods from T_h-SF measurements was called T_d-

SF-ET_{sim}, T_d-SF-*Rs*, T_d-SF-ETo and T_d-SF-ETp, while the T_d estimated from T_h-TSEB estimations was called T_d-TSEB-ET_{sim}, T_d-TSEB-*Rs*, T_d-TSEB-ETo and T_d-TSEB-ETp, respectively.

3 Results

3.1 Biophysical traits and physiological measurements

Table 1 shows an analysis of variance (ANOVA) of the main biophysical traits and Table 2 the average of each biophysical variable for each production system and irrigation treatment. The fractional canopy cover (*fc*) significantly varied between production systems, with open vase (MP) and hedgerows presenting the highest and lowest values, respectively. The average *fc* for each production system was 0.56, 0.50 and 0.47 for open vase (MP), central axis and hedgerow, respectively. Canopy height (*hc*) significantly varied between production systems, irrigation treatments and their interaction. Overall, taller trees were observed in the open vase (MP) system. However, open vase (MP) and hedgerow systems led to smaller trees in the severe stress treatment, whereas the central axis had the smallest trees in the mild stress treatment. The measured LAI did not show significant differences among production systems or irrigation treatments.

Variable	Date	PS	TRT	PSxDate	TRTxDate	PSxTRT	PSxTRTxDate
fc	ns	0.008	ns	ns	ns	ns	ns
hc	0.0004	<.0001	<.0001	ns	ns	<.0001	ns
LAI	ns	ns	ns	ns	ns	ns	ns
Ψ_s	ns	0.0059	<.0001	ns	0.0044	0.0398	ns
g_s	ns	ns	<.0001	ns	0.0046	0.0152	ns
E_{leaf}	0.0003	0.0098	<.0001	ns	0.0321	0.0188	ns
T_d-SF	0.0001	0.0033	<.0001	ns	ns	0.0111	ns
T_h-$SF_{morning}$	0.0003	<.0001	<.0001	ns	ns	0.015	ns
T_h-SF_{midday}	ns	ns	<.0001	ns	ns	ns	ns
T_h-$SF_{afternoon}$	ns	0.005	<.0001	ns	0.011	0.001	ns

Table 1. Analysis of variance (three-way ANOVA) testing the effect of date, production system (PS) and irrigation treatment (TRT) and their interaction on fractional canopy cover (*fc*), canopy height (*hc*) and leaf area index (LAI), stem water potential (Ψ_s), and hourly (T_h-SF) and daily transpiration (T_d-SF) measured by sap flow sensors. P values less than 0.05 were considered statistically significant.

Production system	Irrigation treatment	*fc*	*hc*	LAI	T_d-SF
Open Vase	Full irrigation	0.61 a	5.82 a	3.12	4.61 a
	Mild stress	0.57 a	5.42 b	2.8	3.8 ab
	Severe stress	0.51 a	5.01 c	2.96	1.3 c
Central Axis	Full irrigation	0.53 ab	4.11 d	3.08	3.75 b
	Mild stress	0.5 ab	4.07 d	3.27	2.6 b
	Severe stress	0.48 ab	3.5 e	3.16	1.54 c
Hedgerow	Full irrigation	0.44 b	4.02 d	2.61	3.37 b
	Mild stress	0.5 b	4.78 c	3.7	3.59 b
	Severe stress	0.49 b	4.18 d	3.65	0.99 c

Table 2. Comparison of fractional canopy cover (*fc*), canopy height (*hc*) and leaf area index (LAI), and daily transpiration (T_d-SF) measured during the flight campaign. Different letters mean significant differences at $p < 0.05$ using Tukey's honest significant difference test considering the interaction between production system and irrigation treatment.

3.1.1 Stem water potential, stomatal conductance and leaf transpiration

The diurnal patterns of Ψ_s, g_s, and E_{leaf} exhibited variations primarily attributed to the irrigation treatment (Fig. 3). These variations led to significant differences in tree daily average Ψ_s, g_s, and E_{leaf} among the different irrigation treatments (Table 1). Moreover, the interaction between production system and irrigation treatment (PSxTRT) had a significant impact, primarily attributable to the central axis subjected to the mild stress treatment. The central axis under the mild stress treatment exhibited values comparable to those observed in the severe stress treatment. The daily pattern of Ψ_s exhibited significant differences between irrigation treatments as early as 7:00 hours. In contrast, discernible significant differences between irrigation treatments for g_s and E_{leaf} were evident as early as 9:00 hours. Differences in Ψ_s, g_s and E_{leaf} between irrigation treatments remained evident until 16:00 hours. The peak disparities in Ψ_s, g_s and E_{leaf} among irrigation treatments were observed around 12:00 hours. During this time, Ψ_s had its most reduced values with an average of -1.35 MPa in the full irrigation, -1.86 MPa in the mild stress and -2.30 MPa in the severe stress treatments. Simultaneously, g_s attained its maximum values with an average of 0.41 mol m^{-2} s^{-1}, 0.25 mol m^{-2} s^{-1}, and 0.12 mol m^{-2} s^{-1} for the full irrigation, mild stress, and severe stress treatments, respectively. The most pronounced variations in E_{leaf} among irrigation treatments occurred at 12:00 hours, and the highest E_{leaf} values were recorded at 14:00 hours, with respectively averaged values of 10.61 mmol m^{-2} s^{-1}, 6.96 mmol m^{-2} s^{-1} and 5.24 mmol m^{-2} s^{-1} for the full irrigation, mild stress and severe stress treatments. Finally, on average, the tree daily mean Ψ_s for the fully irrigated treatment was -1.18 MPa, while the mild stress and severe stress treatments showed values of -1.65 MPa and -1.99 MPa, respectively. Similarly, the tree daily averaged values of g_s were 0.32 mol m^{-2} s^{-1}, 0.21 mol m^{-2} s^{-1}, and 0.13 mol m^{-2} s^{-1} for full irrigation, mild stress, and severe stress treatments, respectively. Additionally, the tree daily E_{leaf} values were 7.74 mol m^{-2} s^{-1}, 5.77 mol m^{-2} s^{-1}, and 4.12 mol m^{-2} s^{-1} for full irrigation, mild stress, and severe stress treatments, respectively.

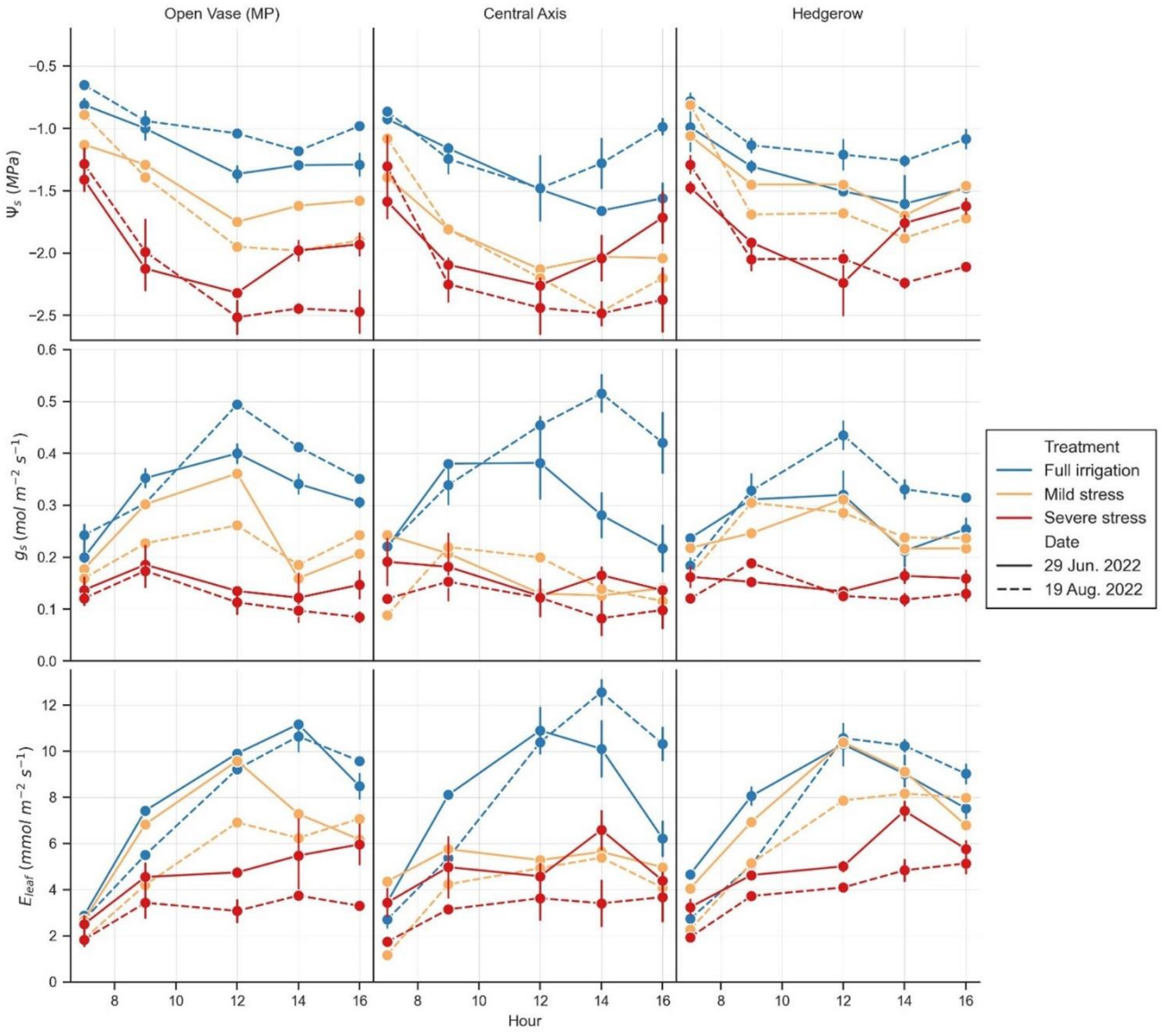

Figure 3: Daily course of stem water potential (Ψ_s), stomatal conductance (g_s) and leaf transpiration (E_{leaf}) for 29th June and 19th August 2022 in almond trees with three different production systems (open vase (MP), central axis and hedgerow) and irrigation treatments (full irrigation, mild stress, and severe stress).

3.1.2 Sap flow transpiration

The T_d-SF showed significant differences among production systems, irrigation treatments, PSxTRT and dates (Table 1). The open vase (MP) transpired significantly higher, with an average of 3.13 mm d^{-1} compared to 2.64 mm d^{-1} for the central axis

and 2.46 mm d^{-1} for the hedgerow systems. Notably, in hedgerow, the mild stress treatment showed higher T_d-SF values compared to the full irrigation treatment, although the difference was not statistically significant (Table 2).

Figure 4 shows the daily patterns of T_h-SF. The T_h-SF patterns exhibited variations based on production system, irrigation treatment, and date. The daily pattern may vary between days due to differences in the main weather forcing parameters (see Fig. 2), as well as an irrigation scheduling error that occurred on June 29th at 12:00 hours, coinciding with the ongoing measurements. The error in the irrigation schedule resulted in significant pattern variations, particularly in the severe stress treatment. In this treatment, T_h-SF exhibited a notable increase at 13:00 hours, reaching its peak at 14:00 and 15:00 hours on June 29th in all production systems. The maximum T_h-SF rates recorded in the severe stress treatment on June 29th were 0.14 mm h^{-1}, 0.20 mm h^{-1}, and 0.23 mm h^{-1} for the open vase (MP), central axis, and hedgerow systems, respectively. Conversely, the maximum T_h-SF rates in the severe stress treatment on August 29th were observed between 10:00 and 12:00 hours, with 0.10 mm h^{-1}, 0.12 mm h^{-1}, and 0.07 mm h^{-1} for the open vase (MP), central axis, and hedgerow systems, respectively.

In the full irrigation treatment, the maximum T_h-SF rates varied depending on the day and the production system, occurring between 12:00 and 14:00 hours. In the open vase (MP) system, the highest T_h-SF values, averaging 0.45 mm h^{-1}, were recorded at 14:00 hours. In the central axis system under full irrigation, the maximum T_h-SF occurred at 12:00 hours on June 29th and at 14:00 hours on August 19th, with a T_h-SF rate of 0.43 mm h^{-1} for both dates. In the hedgerow system, the full irrigation treatment yielded a maximum T_h-SF of 0.37 mm h^{-1} on both days, observed at 12:00 hours on June 29th and at 14:00 hours on August 19th.

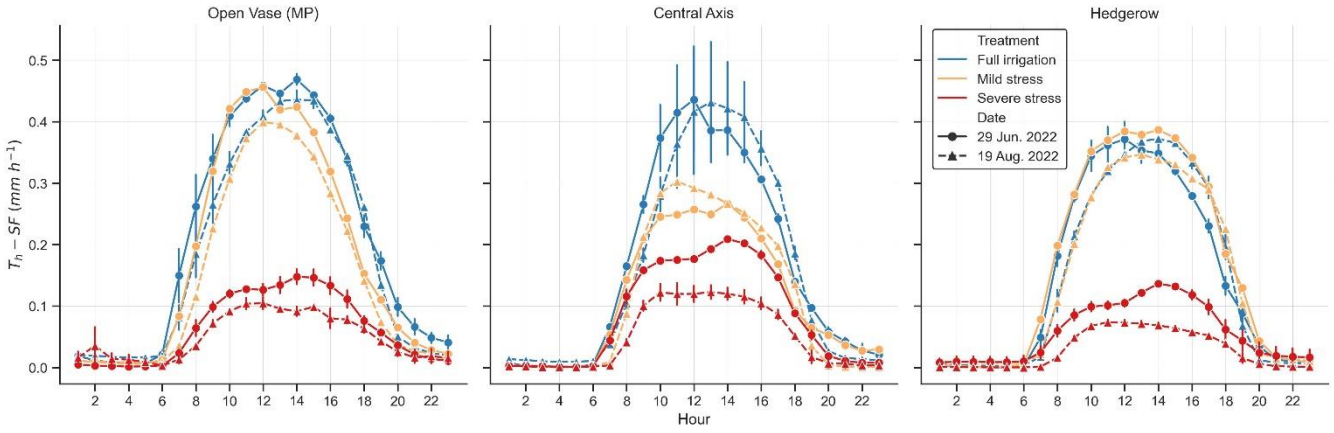

Figure 4: Daily course of hourly sap flow transpiration (T_h-SF) for different irrigation treatments in the production systems a) open vase (MP), b) central axis, and c) hedgerow, for dates 29th June and 19th August 2022.

Similar to the full irrigation treatment, in the mild stress treatment, the timing of maximum T_h-SF depended on the day and the production system. In the mild stress treatment for the open vase (MP), the maximum T_h-SF was recorded at 12:00 hours, corresponding to 0.45 mm h^{-1} on June 29th and 0.39 mm h^{-1} on August 19th. In contrast, the mild stress treatment for the central

axis system reached its peak at 14:00 hours on June 19th and at 12:00 hours on August 19th, with T_h-SF rates of 0.26 mm h^{-1} and 0.30 mm h^{-1}, respectively. In the hedgerow system, under the mild stress treatment, the maximum T_h-SF rates of approximately 0.38 mm h^{-1} and 0.34 mm h^{-1} were observed at 14:00 hours on June 29th and at 12:00 hours on August 19th, respectively.

The T_h-SF exhibited significant differences between 6:00 and 21:00 hours, attributed to the irrigation treatments. T_h-SF for the severe stress treatment was systematically lower than the other two treatments. These differences were more evident during daytime hours. Thus, the maximum differences between the full irrigation and severe stress treatments were observed at 12:00 hours, reflecting an averaged difference of 0.28 mm h^{-1}. Furthermore, nocturnal fluxes, which accounted for approximately 5% of the total T_d-SF, were observed, with the exception of one tree in the open vase (MP) and one tree in the hedgerow system (both under the severe stress treatment) where nocturnal T_h-SF contributed to 21.3% and 10.6% of the total T_d-SF, respectively. The statistical analysis showed that T_h-SF during the morning (6:00 to 10:00 hours) and afternoon (14:00 to 18:00 hours) showed significant differences among production systems and PSxTRT (Table 1). During those daytime intervals, the open vase (MP) production system demonstrated significantly higher T compared to the other production systems. The significance of PSxTRT is explained by the fact that the hedgerow, under the mild stress treatment, exhibited higher T_h-SF values than the full irrigation treatment in both time periods. Notably, although there was no statistical difference between production systems at midday (11:00 to 13:00 hours), the irrigation treatment was significant for mean T_d-SF (Table 1).

Figure 5 illustrates the relationship between the T_h-SF measured during the days of the flight campaign and the key parameters utilized in the estimation of T_d (*Rs*, ETo, and ETp) for all irrigation treatments. T_h-SF was strongly correlated with *Rs*, ETo and ETp for all irrigation treatments. Overall, the relationship between T_h-SF and ETo had the highest Pearson correlation coefficient (*r*), with values of 0.95, 0.95 and 0.90 for the full irrigation, mild stress and severe stress treatments, respectively. Similarly, the correlation with *Rs* yielded *r* values of 0.94, 0.94, and 0.87, while ETp showed *r* values of 0.94, 0.94, and 0.85, respectively for the full irrigation, mild stress, and severe stress treatments. The ETp model exhibited a root mean squared error (RMSE) of 0.22 mm h^{-1} compared to T_h-SF for the full irrigation treatment. Additionally, the RMSE of the ETp model showed significant variation between production systems, with an error of 0.18 mm h^{-1} for the open vase (MP), 0.19 mm h^{-1} for the central axis, and 0.27 mm h^{-1} for the hedgerow systems.

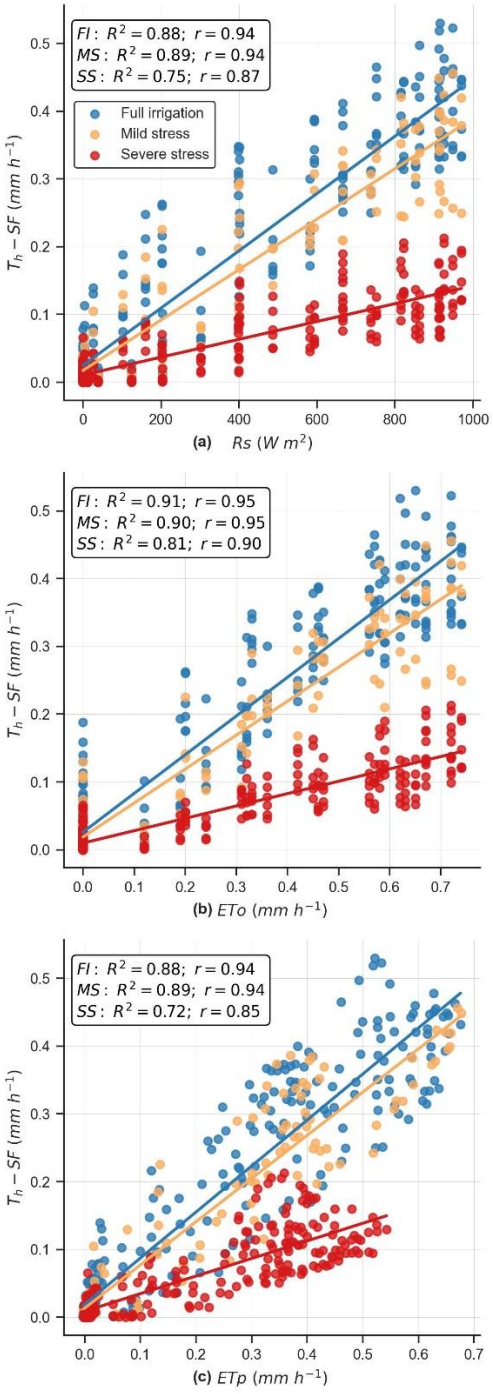

Figure 5: Regression between hourly sap flow transpiration (T_h-SF) with a) solar irradiance (*Rs*), b) reference evapotranspiration (ETo) and c) potential evapotranspiration (ETp), separating by irrigation treatment. The box displays the statistical values for the determination coefficient (R^2) and Pearson's correlation coefficient (*r*) across the full irrigation, mild stress, and severe stress treatments.

The difference between the hourly and daily ratio of *Rs* ($\%_{RS}$), ETo ($\%_{ETo}$) and ETp ($\%_{ETp}$) and T-SF is shown in Fig 6. The diurnal pattern in $\%_{RS}$ was significantly different between irrigation treatments, but not in production systems. The $\%_{RS}$ displayed a relatively consistent trend between 9:00 and 15:00, fluctuating within the range of 28 to 58% primarily influenced by irrigation treatment and date. However, during the interval from 12:00 to 15:00, the $\%_{RS}$ did not show significant differences across production systems, irrigation treatments and dates. During this interval of time, the overall average values of $\%_{RS}$ were -14.47, -15.70, -10.2 and -2.47% from 12:00 to 15:00 hours, respectively.

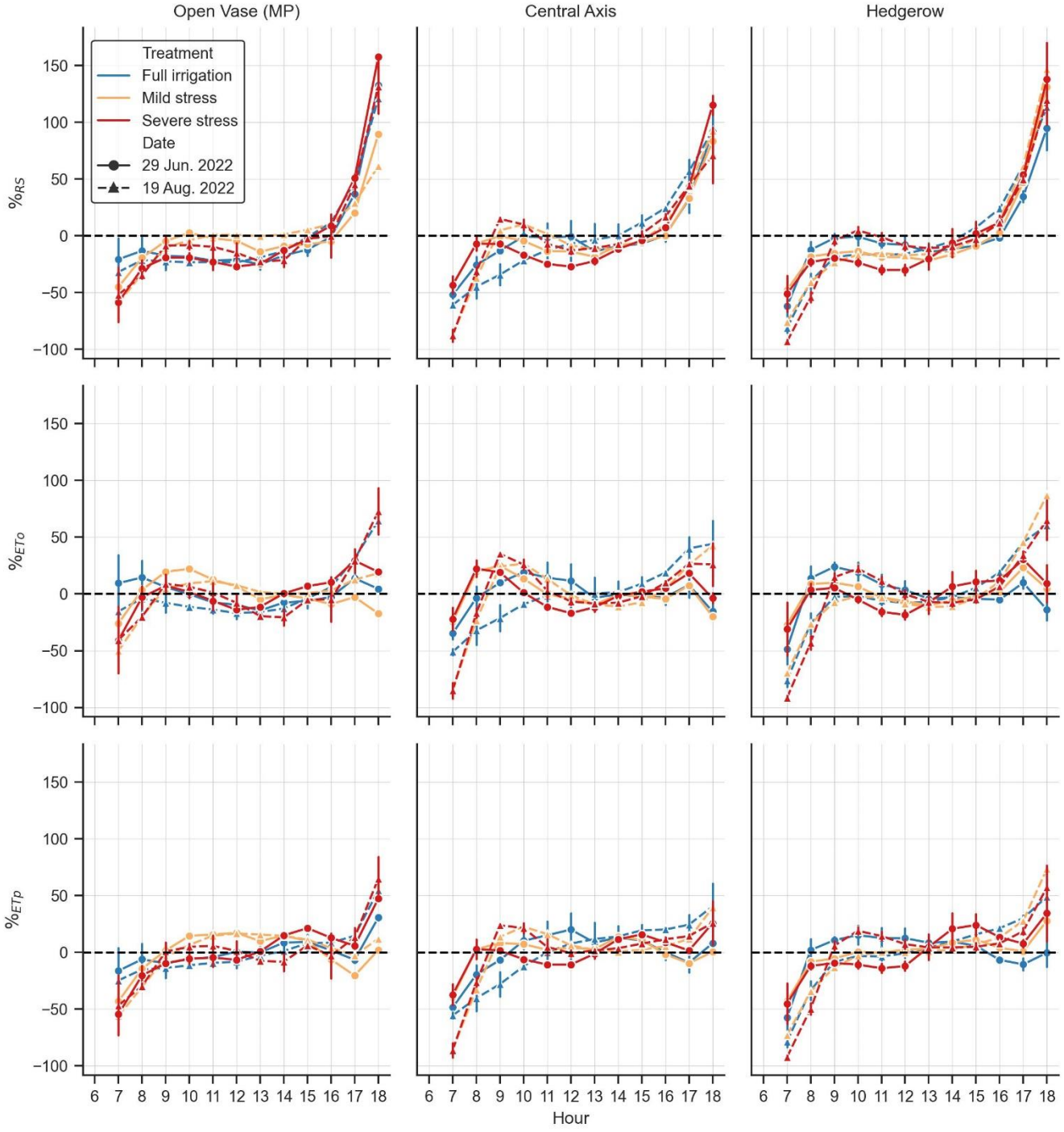

Figure 6. Daily evolution of difference between hourly and daily mean of αRS, αET$_o$ and αET$_p$. α represents the ratio between transpiration and the reference variable, while '%' corresponds to the formula $100 \times (\alpha_{Hour} - \alpha_{Day}) / \alpha_{Day}$, where the subindex indicates the respective method.

For its part, $\%_{ETo}$ exhibited a distinct diurnal pattern between the two dates. Values remained relatively constant between 9:00 and 16:00, ranging from -16.44% to 18.06% on both dates. Similar to $\%_{RS}$, $\%_{ETo}$ showed no significant differences between irrigation treatment and date from 12:00 to 14:00 hours. During this time interval, the mean $\%_{ETo}$ values were -4.87% at 12:00, -8.52% at 13:00, and -4.71% at 14:00. The interaction between irrigation treatment and date began to display significant differences from 14:00 to 18:00, with the severe stress treatment on June 29th showing significantly higher values. On the other hand, the $\%_{ETp}$ pattern exhibited significant variations depending on irrigation treatment and date from 7:00 to 10:00 hours, and after 17:00 hours. However, between 11:00 and 16:00 hours, $\%_{ETp}$ did not exhibit any significant effects attributed to production system, irrigation treatment, or date. Between 11:00 and 16:00 hours, $\%_{ETp}$ ranged from -1.16% to 13.07%, with the minimum percentage difference recorded at 11:00 hours (1.16%) on June 29th and 12:00 hours (3.10%) on August 19th.

Figure 7 shows the relative RMSE (RRMSE) and bias (Rbias) when estimating T_d from T_h-SF. The T_d-SF-EF_{sim} exhibited an RRMSE ranging from 2.7% to 26% after 7:00 hours. Overall, the lowest RRMSE for T_d-SF-EF_{sim} was observed at 14:00 hours. However, the RRMSE of T_d-SF-EF_{sim} showed significant variability among irrigation treatments at this time, with values of 8.22%, 5.28 % and 17.4 % for the full irrigation, mild stress and severe stress treatments, respectively. Conversely, the RRMSE of T_d-SF-EF_{sim} varied as a function of date in the severe stress treatment after 12:00 hours. While on June 29th the RRMSE decreased, on August 19th it increased with values of 26.14% at 14:00 and 25.36% at 16:00 hours, respectively.

The RRMSE of T_d-SF-*Rs* and T_d-SF-ETo varied with irrigation treatment. In the full irrigation and mild stress treatments, the RRMSE of T_d-SF-*Rs* showed a convex shape throughout the day, with higher values in the early morning and late afternoon. In the full irrigation treatment, the RRMSE of T_d-SF-*Rs* steadily decreased until 15:00 hours, reaching an average minimum value of 8.4%. In the mild stress treatment, the RRMSE of T_d-SF-*Rs* remained relatively constant at around 10% between 9:00 and 16:00, reaching its lowest point at 15:00 (RRMSE of 4.18%). In the severe stress treatment, the RRMSE of T_d-SF-*Rs* exhibited a sinusoidal curve pattern. In this treatment, the RRMSE of T_d-SF-*Rs* hovered around 15.3% at 9:00 and began to increase until 12:00 or 13:00 hours, with a mean RMSE ranging between 29.83% and 34% depending on the date. On both dates, the RRMSE of T_d-SF-*Rs* decreased at 15:00, with an RMSE of 7.37% and 12.08% on June 29th and August 19th, respectively.

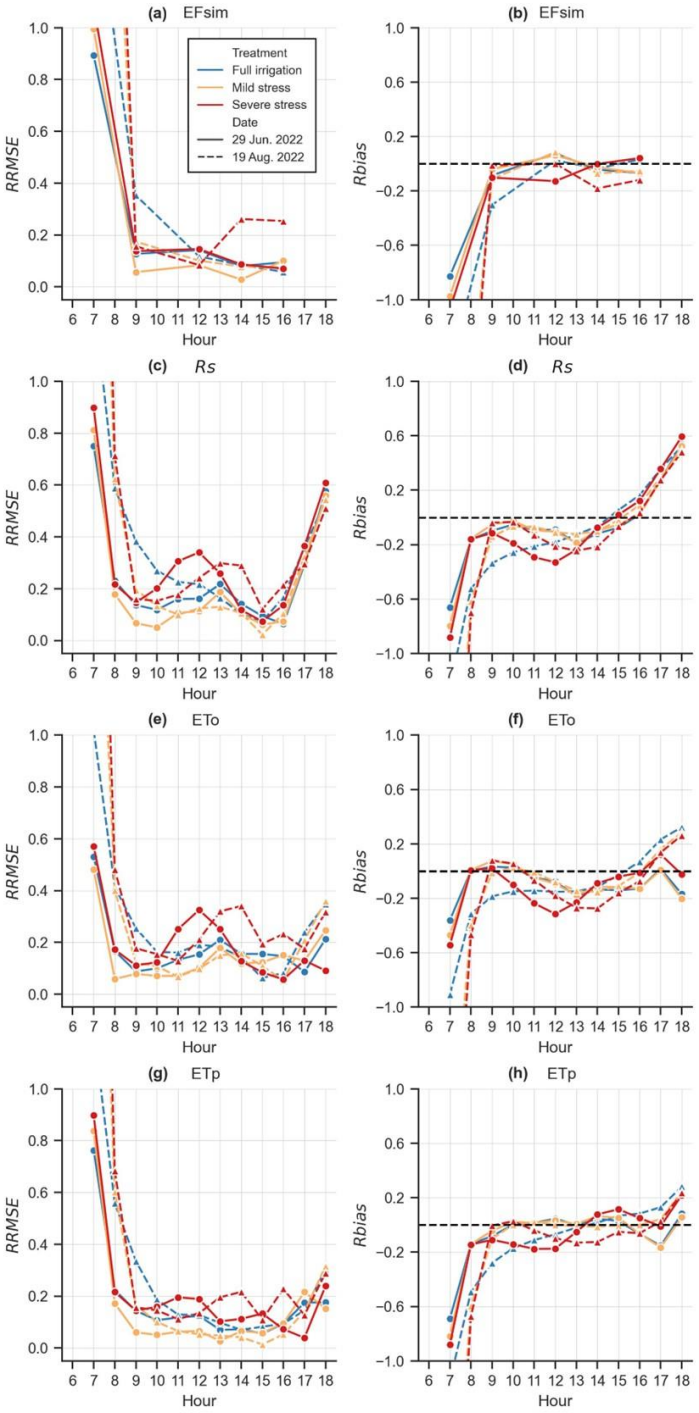

440

Figure 7. Relative RMSE (RRMSE) and bias (Rbias) calculated for daily transpiration estimates obtained through the EF_{sim}, *Rs*, ETo, and ETp methods using T_h-SF at the time when ETo was greater than 0 mm h^{-1}.

The time at which the minimum RRMSE of T_d-SF-ETo occurred varied depending on the interaction between irrigation treatment and date. In the full irrigation treatment, the lowest RRMSE of T_d-SF-ETo, corresponding to 8.59%, was observed at 17:00 on June 29th. Conversely, in the full irrigation treatment, the minimum RRMSE of T_d-SF-ETo (6.29%) was recorded at 15:00 on August 29th. For the mild stress treatment, the minimum RRMSE of T_d-SF-ETo on June 19th was 5.86% and was recorded at 8:00, while the minimum RRMSE of T_d-SF-ETo on August 29th was observed at 16:00, corresponding to 5.27%. Similar to T_d-SF-*Rs*, the RRMSE of T_d-SF-ETo in the severe stress treatment presented a sinusoidal curve. The RRMSE of Td-SF-ETo decreased until approximately 10:00 or 11:00 before gradually increasing around noon. On June 29th, it reached a maximum value of 32.50% at 12:00. After 12:00, the RRMSE of T_d-SF-ETo began to decrease and reached 5.70% at 16:00 hours. On August 29th, a maximum RRMSE of T_d-SF-ETo was observed at 14:00 hours, reaching 34.01%, whereas the minimum RRMSE of T_d-SF-ETo was recorded at 11:00 (RRMSE of 12.83%). Finally, the RRMSE of T_d-SF-ETp exhibited higher values in the early morning and late afternoon but remained constant from 9:00 to 17:00. Although the severe stress treatment exhibited the highest RMSE of T_d-SF-ETp, no significant differences were detected among production systems, irrigation treatments or dates. Overall, the minimum RRMSE of T_d-SF-ETp of 7.51% was recorded at 15:00 hours.

3.2 Regression of measured and remotely estimated T_h with the TSEB-2T

Figure 8 shows the concurrence between T_h-TSEB and T_h-SF. The most accurate estimation was obtained at 14:00 hours, with an RRMSE of 29% and an R^2 value of 0.81. Comparable error statistics were obtained at 12:00 hours, with an RRMSE of 39% and an R^2 value of 0.71. The least favorable outcomes were observed during early morning flights, specifically at 7:00 hours, when the TSEB-2T model provided null estimations for multiple trees. Overall, T_h-TSEB showed an overestimation at all hours. However, these overestimations were more pronounced at 9:00 and 16:00 hours, which respectively corresponded to RRMSE values of 77% and 59%.

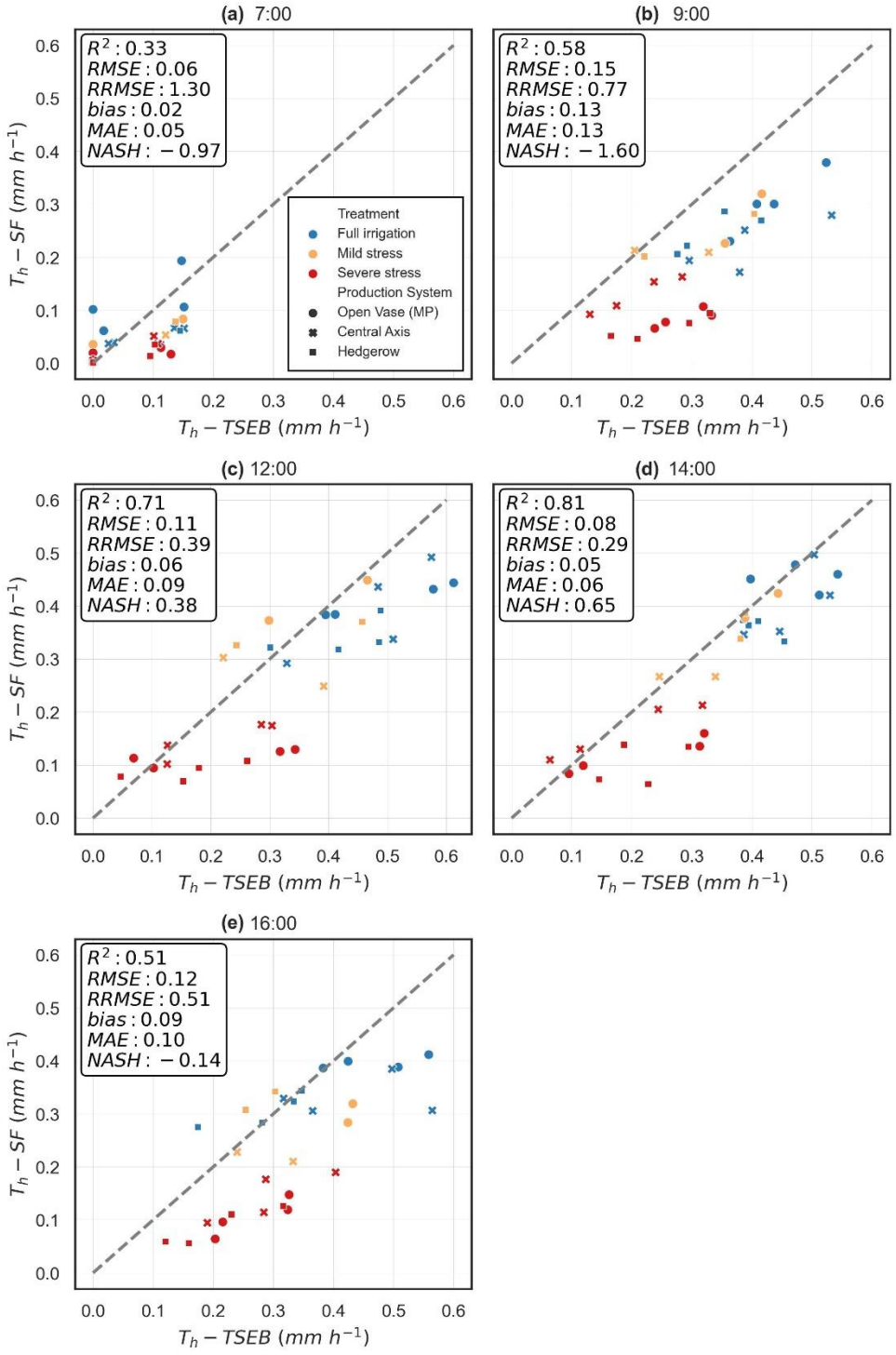

465

Figure 8. Regressions between measured and estimated hourly transpiration with the TSEB-2T model and high-resolution images by hour, production system and irrigation treatment.

Table 3 presents an ANOVA analysis aimed at assessing the sensitivity of T_h-TSEB to production system, irrigation treatment, and date. The estimations of T_h-TSEB indicated significant differences among irrigation treatments across all flight times. The three irrigation treatments could be differentiated using the estimations at 9:00, 12:00 and 14:00 hours. On the other hand, the T_h-TSEB at 7:00 hours in the mild stress treatment presented similar values compared with the full irrigation treatment. At 16:00 hours, the mild stress treatment showed comparable T_h-TSEB estimations with the full irrigation and severe stress treatments. The production system presented important differences in T_h-TSEB when considering the flights conducted at 9:00 and 16:00 hours. At these times, the open vase (MP) production system exhibited significantly higher T_h-TSEB. In contrast, the flights conducted at 7:00, 12:00 and 14:00 hours estimated similar T_h-TSEB values between production systems.

Hour	Date	PS	TRT	PSxDate	TRTxDate	PSxTRT	PSxTRTxDate
7:00	<.0001	ns	0.0032	ns	0.0282	ns	ns
9:00	<.0001	0.0062	<.0001	ns	ns	ns	ns
12:00	<.0001	ns	<.0001	ns	ns	ns	ns
14:00	0.002	ns	<.0001	ns	ns	ns	ns
16:00	ns	0.012	0.0032	ns	ns	ns	ns

Table 3. Analysis of variance (three-way ANOVA) testing the effects of date, production system (PS) and irrigation treatment (TRT) on T_h-TSEB for each hour of flight conducted.

Table 4 shows the influence of production system, irrigation treatment and date on the squared error of T_h-TSEB compared with T_h-SF. The results indicate that T_h-TSEB using the flight performed at 7:00 hours on June 29th exhibited a systematic error, generating important differences in the squared error due to the date. Furthermore, the squared error showed significant differences between irrigation treatments only for the flights conducted at 9:00. Additionally, a significant effect attributed to the interaction of production system and irrigation treatment was observed at 9:00 hours. Notably, the open vase (MP) under severe stress treatment exhibited a higher error at 9:00 hours. Moreover, while the production system, treatment, and date did not have a significant impact on the RMSE of T_h-TSEB for flights conducted at 12:00, 14:00, and 16:00 hours (Table 4), it is noteworthy that the severe stress treatment consistently exhibited a higher error across all flight hours (Table 5).

Hour	Date	PS	TRT	PSxDate	TRTxDate	PSxTRT	PSxTRTxDate
7:00	0.0004	ns	ns	ns	ns	ns	ns
9:00	ns	ns	0.0386	ns	ns	0.0087	ns
12:00	ns	ns	ns	ns	ns	ns	ns
14:00	ns	ns	ns	ns	ns	ns	ns
16:00	ns	ns	ns	ns	ns	ns	ns

Table 4. Analysis of variance (three-way ANOVA) evaluating the effects of date, production system (PS) and irrigation treatment (TRT) on the root mean squared error (RMSE) of T_h-TSEB for each hour of flight conducted.

Treatment	7:00	9:00	12:00	14:00	16:00
Full irrigation	0.059	0.142 ab	0.106	0.069	0.104

Treatment	7:00	9:00	12:00	14:00	16:00
Mild stress	0.049	0.096 b	0.089	0.037	0.093
Severe stress	0.057	0.167 a	0.113	0.105	0.15

Table 5. Root mean squared error (RMSE) of T_h-TSEB (mm h^{-1}), categorized by irrigation treatment, for each hour of flight conducted.

3.3 Evaluation of daily upscaling methods to estimate T_d with the TSEB-2T

The T_d was estimated using the different upscaling methodologies and with the 14:00 hours T_h-TSEB estimation as starting point (Fig. 9). The T_h-TSEB at 14:00 hours was selected due to the highest accuracy obtained (Fig. 8) when validated against the T_h-SF. Overall, the results indicate that the EF_{sim}, *Rs* and ETo upscaling methods yielded similar results, even reducing the RRMSE obtained by T_h-TSEB. In contrast, the ETp methods exhibited higher RMSE than those obtained by T_h-TSEB. The T_d-TSEB-*Rs* and T_d-TSEB-ETo reached the highest accuracy, showing an RMSE (RRMSE) of 0.62 mm d^{-1} (23%) and 0.61 mm d^{-1} (22%), respectively. The T_d-TSEB-EF_{sim} and T_d-TSEB-ETp approaches had RMSE (RRMSE) values of 0.72 mm d^{-1} (26%) and 0.89 mm d^{-1} (32%), respectively. In addition, the T_d-TSEB-EF_{sim} and T_d-TSEB-ETp yielded larger overestimations, with biases of 0.38 mm d^{-1} and 0.61 mm d^{-1}, compared to T_d-TSEB-*Rs* and T_d-TSEB-ETo, which had biases of 0.22 mm d^{-1} and 0.14 mm d^{-1}.

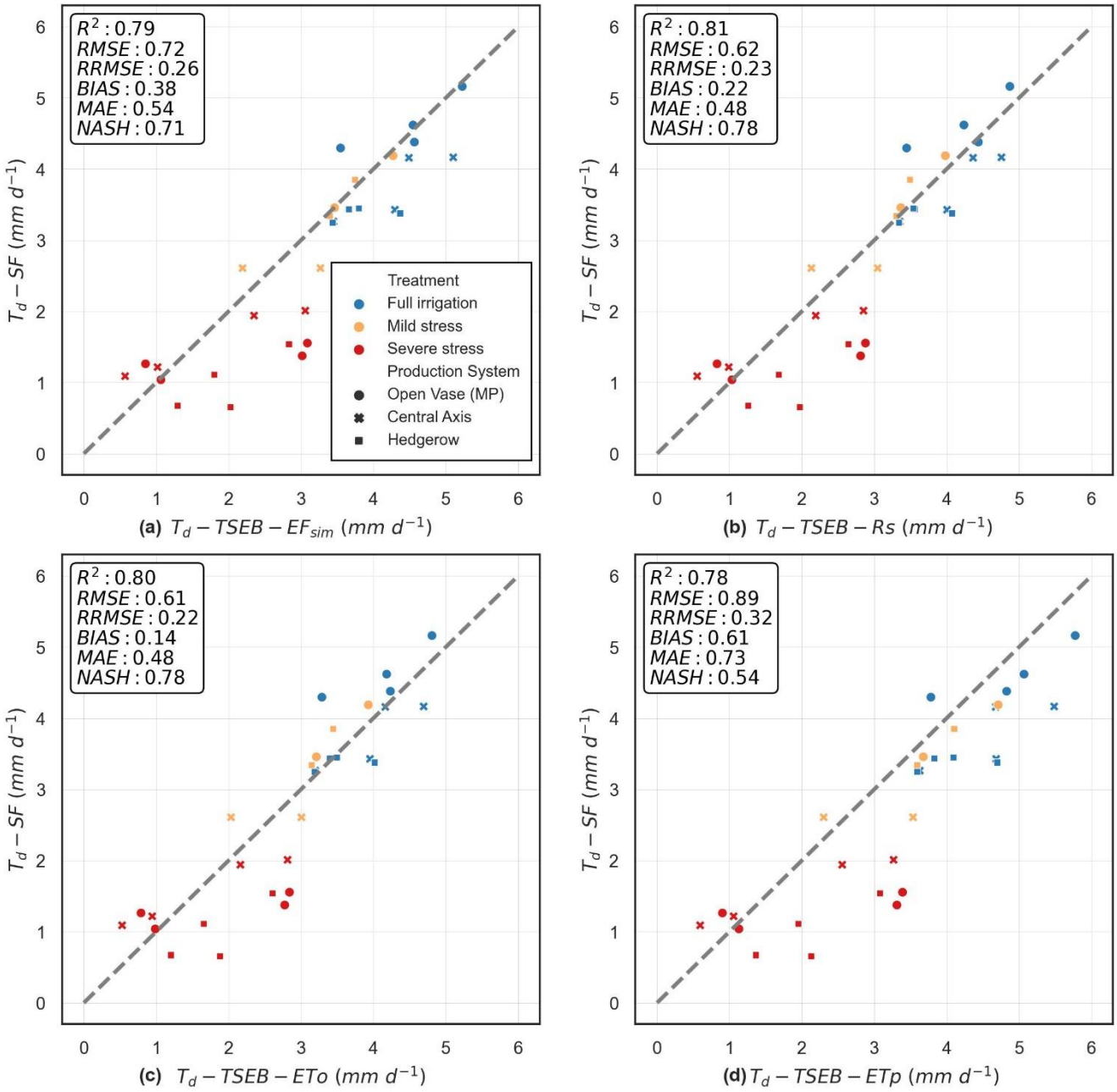

Figure 9. Regressions between measured (T_d-SF) and estimated daily transpiration (T_d-TSEB) by production system and irrigation treatment with the following upscaling methodologies: a) EF_{sim}, b) *Rs* c) ETo, and d) ETp.

510

Table 6 shows an ANOVA analysis performed to detect the sensitivity of T_d-TSEB-EF_{sim}, T_d-TSEB-*Rs*, T_d-TSEB-ETo and T_d-TSEB-ETp to irrigation treatment, production system and date. The results indicate that all approaches exhibited significant

differences in the estimated T_d attributed to irrigation treatment and date. Finally, an ANOVA analysis was conducted to assess the influence of each upscaling method on the RMSE, considering production system, irrigation treatment and date (Table 7). The RMSE in T_d-TSEB-EF_{sim}, T_d-TSEB-*Rs*, T_d-TSEB-ETo and T_d-TSEB-ETp varied significantly due to irrigation treatment. All the daily upscaling methods resulted in significantly higher RMSE values in the severe stress treatment (Table 8).

Model	Date	PS	TRT	PSxDate	TRTxDate	PSxTRT	PSxTRTxDate
T_d-TSEB-EF_{sim}	0.0002	ns	<.0001	ns	ns	ns	ns
T_d-TSEB-*Rs*	0.0007	ns	<.0001	ns	ns	ns	ns
T_d-TSEB-ETo	0.0003	ns	<.0001	ns	ns	ns	ns
T_d-TSEB-ETp	0.0252	ns	<.0001	ns	ns	ns	ns

Table 6. Analysis of variance (three-way ANOVA) for the evaluation of the effects of date, production system (PS) and irrigation treatment (TRT) on T_d estimated with TSEB-2T using flights conducted at 14:00 hours and EF_{sim}, *Rs*, ETo and ETp upscaling methods. P values less than 0.05 were considered statistically significant.

Model	Date	PS	TRT	PSxDate	TRTxDate	PSxTRT	PSxTRTxDate
T_d-TSEB-EF_{sim}	ns	ns	0.0071	ns	ns	ns	0.0375
T_d-TSEB-*Rs*	ns	ns	0.0094	ns	ns	ns	ns
T_d-TSEB-ETo	ns	ns	0.0183	ns	ns	ns	ns
T_d-TSEB-ETp	ns	ns	0.0420	ns	ns	ns	0.0416

Table 7. Analysis of variance (three-way ANOVA) evaluating the effects of date, production system (PS) and irrigation treatment (TRT) on the root mean squared error (RMSE) of T_d estimated with TSEB-2T using flights conducted at 14:00 hours and EF_{sim}, *Rs*, ETo and ETp upscaling methods. P values less than 0.05 were considered statistically significant

Irrigation treatment	EF_{sim}	*Rs*	ETo	ETp
Full irrigation	0.55 b	0.43 b	0.44 b	0.66 ab
Mild stress	0.32 b	0.32 b	0.37 b	0.42 b
Severe stress	0.97 a	0.85 a	0.83 a	0.92 a

Table 8. Root mean squared error (RMSE, mm d^{-1}) of the estimated T_d using the TSEB-2T and EF_{sim}, *Rs*, ETo and ETp upscaling approaches by irrigation treatment. Different letters mean significant differences at $P < 0.05$ using Tukey's honest significant difference test considering the irrigation treatments.

4 Discussion

The timing of measurements is crucial for determining the level of water stress and accurately estimating T fluxes. Our observations indicate that the highest differences in Ψ_s, g_s, E_{leaf}, and T_h-SF between irrigation treatments were near solar noon (between 11:00 and 14:00 hours), underlining the importance of considering diurnal variations in plant responses to water stress. This period is often when water stress is most pronounced, and plant physiological processes are most affected. Accurate measurements during this critical time frame can provide valuable insights into the impact of water stress on plant behavior and T rates. Therefore, our findings reinforce the conclusion that the best moment to determinate water stress is noon or early

afternoon, considering the maximum peaks of T (Gentine et al. 2007; Delogu et al. 2012) and the maximum differences between water status (Bellvert et al. 2014; Anderson et al. 2021; Tian and Schreiner 2021).

In addition, the T_h-TSEB estimated using images obtained at 12:00 and 14:00 hours yielded the most accurate results and were able to detect greater differences between irrigation treatments, while the irrigation treatment did not significantly affect the RMSE (Tables 3 and 4). This is in line with the findings of Anderson et al. (2021), who showed how earlier overpasses often created uniform maps of ET without differentiating between crop water demand. Additionally, Bellvert et al. (2014) showed that the optimal time for capturing high-resolution thermal images to minimize shade effects and monitor leaf water potential and T_c is around solar noon. The higher overestimations in T_h-TSEB estimated using images obtained at 7:00, 9:00 and 16:00 hours could be explained by the shadow that covered the thermal images. The thermal images captured at 7:00, 9:00 and 16:00 hours were more susceptible to thermal radiation directionality (TDR) and shadow effects resulting from the higher zenith angle of the sun. Moreover, the significant contrast between inter-row soil and canopy leads to considerable directional variability in the thermal images (Mwangi et al., 2023). Although TSEB-2T accounts for radiation directionality when estimating *H* (Norman et al., 1995) and shortwave transmittance (Parry et al., 2019), it may still be susceptible to shadow effects because it does not distinguish between sunlit and shaded sources. To address this issue, Mwangi et al., (2022) proposed a four-component scheme (SPARSE4) as an option to account for sunlit/shaded soil/vegetation energy sources. This scheme couples a dual-source energy balance (SPARSE) model with the physically based unified four-component radiative transfer (UFR97) model. However, The T_h-TSEB model demonstrates effective differentiation between irrigation treatments at all hours, particularly around solar noon, where differences between all irrigation treatments are evident. Conversely, it is noteworthy that T_h-TSEB fails to exhibit significant differences between production systems around solar noon (Table 3). This poses a challenge when estimating T_d using upscaling methods, as no model detected variations in T_d by production system, as evidenced by T_d-SF (Table 6). This limitation is especially critical when estimating T_d from T_h-TSEB in canopies with diverse architectural structures.

While the comparison between actual T_d-SF and T_d-TSEB-EF_{sim}, T_d-TSEB-*Rs*, T_d-SEB-ETo and T_d-TSEB-ETp showed similar results (Fig. 9), T_d-TSEB-*Rs*, T_d-SEB-ETo enhanced the accuracy of T_d estimates, which is reflected in the reduced RMSE values of 0.62 mm d^{-1} and 0.61 mm d^{-1}, respectively. It should be noted that both Cammalleri et al. (2014) and Nassar et al. (2021) reported the R_S method as yielding the best results when used as an upscaling parameter to estimate daily ET. However, our results suggest that the superior performance of *Rs* and ETo to estimate T_d can be attributed to their capacity to rectify the overestimation observed in T_h-TSEB estimates, rather than their inherent alignment with the T_h-SF pattern. The underestimation is clarified by the $\%_{RS}$ at 14:00 hours, which ranged from -2.47% to -14.47%, while the $\%_{ETo}$ ranged from -4.71% to -8.52% (Fig. 6). Related to our results, Van Niel et al. (2012) and Cammalleri et al. (2014) observed a systematic underestimation of estimated daily ET values using the *Rs* approach for a wide range of ecosystems and weather conditions. In this regard, Anderson et al. (1997) proposed a correction factor of 1.1 to compensate for systematic bias, increasing by 10% the daily ET estimations. Among the advantages of the *Rs* method, Cammalleri et al. (2014) highlighted its uniform bias around the acquisition time and throughout the season, in contrast to the EF method, ETo, and the top-of-atmosphere radiance (RTOA)

as reference variables. Nassar et al. (2021) also found that the *Rs* method exhibits less sensitivity to seasonal and climate variations compared to the EF approach and use of the net radiation-to-solar radiation ratio (*Rn/Rs*). It is important to clarify that both the above cited studies evaluated the EF approach with actual AE measurements using eddy covariance towers as validation data source.

However, our findings indicate that the correction factor proposed by Anderson et al. (1997) of 1.1 for T_d should be determined by water stress, otherwise it may be deemed inadequate. In addition, the timing of the overpass is crucial in determining a correction factor for using the *Rs* and ETo approaches, particularly for trees experiencing water stress. For instance, although the minimum RRMSE of T_d-SF-*Rs* of 10% might be achievable at 15:00 hours, the RRMSE of T_d-SF-*Rs* could reach 25-30% around midday in trees under waters stress. Given the variations of the RRMSE when estimating T_d-SF-*Rs* throughout the day and between days, establishing an appropriate correction factor for water stressed trees presents a challenge. These findings complement those of Cammalleri et al. (2014) and Nassar et al. (2021), who concluded that the *Rs* method is minimally influenced by the timing of the daytime overpass in unstressed vegetation.

The errors associated with the *Rs* and ETo approaches could be attributable to fluctuations in the daily patterns of *Rs*, ETo, and the physiological condition of the tree throughout the day. *Rs* and ETo exhibited an almost perfect concave shape, with their maximum values occurring at 13:00 hours (Fig. 2), which was the local solar noon at our study site. Conversely, in the full irrigation treatment, while stomatal closure was observed at 12:00, both E_{leaf} and T_h-SF either remained steady or even increased until 14:00 hours (Fig. 3 and Fig. 4). The maintenance or increase in E_{leaf} and T_h-SF during the early afternoon can be attributed to the rise in T_a and the decrease in RH, consequently leading to an increase in VPD during the afternoon (Fig. 2). The variation in patterns between *Rs*, ETo, and T_h-SF resulted in lower hourly values of T_h-SF/*Rs* (or T_h-SF/ETo) at midday compared to those observed during the early afternoon (15:00-16:00 hours). On the other hand, T_h-SF/*Rs* (or T_h-SF/ETo) in the early afternoon exhibited more representative values for estimating T_d in the fully irrigated treatment from T_h-SF (Fig. 6). In contrast, the early water stress, as indicated by the Ψ_s, resulted in stomatal closure detected at 9:00 in the severe stress treatment. The impact of stomatal closure can be observed in Fig. 4, where the maximum T_h-SF was achieved before noon in the severe stress treatment, specifically between 10:00 and 12:00 hours. Despite the increase in *Rs* and ETo, the maximum T_h-SF in the severe stress treatment remained nearly constant between 10:00 and 16:00 hours on August 19th. On June 29th, T_h-SF in the severe stress treatment increased rapidly, starting from 12:00 hours and reaching its maximum value at 14:00 hours, similar to the full irrigation treatment. As a result, the disparities between T_h-SF and *Rs* (or ETo) were most pronounced at midday (Fig. 6), leading to significant potential underestimations when using midday measurements. While *Rs* and ETo decreased, T_h-SF remained at its maximum until 16:00 hours. Consequently, the relationship between T_h-SF and *Rs* (or ET_o) started to become more representative of T_d-SF at 15:00 hours on both dates. Therefore, it appears that the optimal time to estimate instantaneous T for daily estimations would fall in the early afternoon, specifically at 15:00 hours, for both the *Rs* and ETo approaches in all irrigation treatments.

Regarding the ETo method, in line with the findings of Cammalleri et al. (2014), using ETo as a reference variable produced results similar to those of the *Rs* method, indicating that it does not represent an improvement. Moreover, the $\%_{ETo}$ pattern

varied from one date to another (Fig. 6), introducing uncertainty into the potential upscaling adjustments. Differences in the $\%_{ETo}$ patterns between days may be attributable to variations in the aerodynamic properties of the canopy between the reference vegetation and the almond canopy. For instance, Colaizzi et al. (2006) obtained good results applying the ETo method in alfalfa and irrigated cotton but poor results for bare soil in drying conditions. It should also be noted that the microclimatic conditions at the location of the weather station may differ from those of the study site, introducing uncertainty into estimation of the actual ETo of the orchard under study. These two issues may be a possible limitation when using ETo as a reference variable to estimate T_d fluxes (Cammalleri et al., 2014).

The EF_{sim} and ETp methods appear to enhance the T_d considering the better and more consistent RRMSE observed throughout the day for T_d-SF-EF_{sim} and T_d-SF-ETp, in contrast to T_d-SF-*Rs* and T_d-SF-ETo. This improvement was also noted in the RRMSE of T_d-TSEB-EF_{sim} and T_d-TSEB-ETp, which performed more similar RRMSE with T_h-TSEB. This suggests that the EF_{sim} and ETp methods induced fewer modification to the error associated with TSEB itself compared to the *Rs* and ETo methods. The improvement of the EF_{sim} method aligns with the daily EF curve observed in previous studies, which does not remain constant but instead exhibits an upward concave shape, especially in non-stressed vegetation (Hoedjes et al., 2008; Delogu et al., 2012; Lhomme and Elguero, 1999; Brutsaert, 1992). Delogu et al. (2012) showed an improvement in the reconstruction of daily ET for various sites and under different climatic conditions, including low water stress, using the EF_{sim} methodology. This is in line with our findings if we consider that their "low water stress" conditions align with the mild stress treatment. However, it should be noted that the RRMSE of T_d-SF-EF_{sim} may increase when using AE estimations during the afternoon for trees under water stress. This is why the RMSE values are significantly higher in T_d-TSEB-EF_{sim} when using the TSEB-2T at 14:00 hours (Table 7). The actual EF shape under water stress during the day differs from the EF_{sim} shape, presenting a flatter profile (Hoedjes et al., 2008; Lhomme and Elguero, 1999). The larger differences between actual EF and EF_{sim} during the afternoon could potentially lead to an underestimation of T_d when using the EF_{sim} method. However, EF_{sim} was able to reduce the RRMSE of T_d-SF-EF_{sim} at noon in the severe stress treatment by up to 15.35% and 17.61% compared to Td-SF-ETo and Td-SF-*Rs*, respectively. Additionally, the T_d-SF-EF_{sim} exhibited 5% less RRMSE than T_d-SF-ETo and T_d-SF-*Rs* in the full irrigation and mild stress treatments. This indicates that the EF_{sim} method might perform well under certain conditions but may have limitations, especially when applied to severely water stressed trees using afternoon measurements.

The remarkable similarity in patterns between ETp and T_h-SF is particularly surprising, considering the concerns raised by Delogu et al. (2012) regarding the applicability of the ETp method under stress conditions. Delogu et al. (2012) suggested that actual ET and ETp might exhibit different daily patterns due to stomatal closure, potentially causing a negative bias when using ETp as a daily upscaling parameter. However, the daily curve of the ratio between T_h-SF and hourly ETp ($\%_{ETp}$) mitigates the sinusoidal shape of $\%_{RS}$ and $\%_{ETo}$, which otherwise increases exponentially from noon to 18:00 hours. Furthermore, the RRMSE of T_d-SF-ETp improves compared to the other methodologies and shows less variability among irrigation treatments and hours compared to using *Rs* and ETo as the adjustment variable. This improvement was particularly evident at 12:00, where T_d-SF-ETp showed approximately 5% less RRMSE in the full irrigation and mild stress treatments, while reducing RRMSE at noon by 10.6% and 12.92% in the severe stress treatment compared to T_d-SF-ETo and T_d-SF-*Rs*, respectively.

Moreover, the ETp model may hold an advantage due to its incorporation of distinct aerodynamic and radiative properties associated with various canopy architectures, which influence the T_h-SF pattern. The variation in RMSE in the estimation of ETp among production systems likely impacted the sensitivity of the ETp model fit to each specific production system. The absence of significant differences in LAI among production systems could affect the accuracy of ETp. Quintanilla-Albornoz et al. (2023) already showed a discrepancy between measured LAI and the fraction of intercepted photosynthetically active radiation (fIPAR) at the study site, where the hedgerow presented higher LAI values but low fIPAR levels. Considering that fIPAR represents 45% of the absorbed light spectrum (Campbell and Norman 1998), these results reinforce the idea of improving the shortwave transmittance model for estimating ET fluxes. Indeed, among the complexities, estimating parameters such as LAI, albedo, and the potential single-leaf stomatal resistance are considered challenging and can pose difficulties in making ETp estimations suitable for operational purposes (Delogu et al. 2012; Gao et al. 2022). However, enhanced ETp models and the refinement of crucial inputs like LAI and albedo can streamline and enhance ETp estimations, further enhancing its utility as a parameter for T_d estimation in trees with different canopy architecture. For instance, implementing a more intricate model to estimate ETp, like the Shuttleworth and Wallace two-source model (Shuttleworth and Wallace, 1985), could enhance the daily upscaling method. This study was conducted over two measurement days with meteorological forcing conditions representative of typical summer days at the study site (Fig. 2). Additional measurement days would allow for the consideration of wider range of meteorological forcing conditions and vegetative stages in almond trees for a more robust assessment of daily T pattern. However, the data collected effectively represent trees under varying levels of water stress (Fig. 3), consistent with the conditions necessary to address the hypothesis of this work.

5 Conclusion

This study evaluates four methodologies to estimate T_d from instantaneous measurements. The daily upscaling methods were evaluated using sap flow measurements in almond trees under three different production systems and three irrigation treatments. Additionally, this study analyzed the daily pattern of physiological parameters, such as a Ψ_s, g_s, E_{leaf} and T_h-SF, to determine the best moment to estimate both T_h and T_d.

The T_h-TSEB model effectively distinguished between irrigation treatments especially at 12:00 and 14:00, when differences between the three irrigation treatments were apparent. However, the T_h-TSEB did not show significant differences between the production systems at that time. Therefore, of the evaluated upscaling methods, none of the models could discern the significant differences in T_d estimates across production systems, as observed in T_d-SF. In addition, the upscaling methodologies were less accurate in severely stressed trees. Especially when using *Rs* and ETo as reference variables, the levels of underestimation exhibited significant variations between irrigation treatments and across different hours. Underestimation was as high as 30% around noon for trees for trees under water stress using the *Rs* and ETo methods. Therefore, it is advisable to carefully choose an appropriate time schedule. In this context, the EF_{sim} and ETp methods

demonstrated more consistent relationships with T_h-SF and mitigated the underestimation observed in all irrigation treatments when using the other methods. For instance, both the ET_{sim} and ETp models reduced the RRMSE by 5% in the full irrigation and mild stress treatments using measurements at 12:00 hours. In the severe stress treatment, EF_{sim} reduced the RRMSE by 17.61%, and 15.25% at noon, while ETp reduced it by 10.6% and 12.92% at noon compared to the *Rs* and ETo methods, respectively.

Moreover, ETp has the advantage of incorporating different aerodynamic and radiative properties associated with production systems. In this sense, the ETp method may be an option to better characterize the T_d in trees with different canopy architectures. In this study, similar LAI estimates between production systems could affect the ETp model, where the hedgerow system showed a significantly higher error. This situation could impact the sensitivity of the ETp model to differentiate T_d between production systems. One approach to enhance T_d estimations could involve refining the Penman-Monteith ETp model and improving the estimations of parameters such as the LAI, albedo, potential single-leaf stomatal resistance, and the shortwave transmittance model. Alternatively, using more sophisticated models, such as the Shuttleworth and Wallace two-source model, could also be considered.

Data availability

All data mentioned in this document have been generated by the IRTA Efficient Use of Water in Agriculture Program team. Data sets produced during this study can be made available upon reasonable request from the corresponding author and/or the Efficient Use of Water in Agriculture Program.

Author contributions

MQ: conceptualization, data curation, formal analysis, investigation, methodology, software, validation, visualization and writing–original draft preparation. JB: conceptualization, funding acquisition, investigation, project administration, supervision, validation and writing–original draft preparation. HN: Software, validation and writing–review & editing. XM: Funding acquisition and writing – review & editing. AP: Data curation and resources.

Competing interests

The contact author has declared that none of the authors has any competing interests.

Disclaimer

Publisher's note: Copernicus Publications remains neutral with regard to jurisdictional claims made in the text, published maps, institutional affiliations, or any other geographical representation in this paper. While Copernicus Publications makes every effort to include appropriate place names, the final responsibility lies with the authors.

Acknowledgements

The authors would like to thank all the Efficient Use of Water in Agriculture program team, at the IRTA, for their technical support, as well as the Horizon 2020 Research and Innovation Program (H2020) of the European Commission, in the context of the Marie Sklodowska-Curie Research and Innovation Staff Exchange (RISE) action and ACCWA project: grant agreement No.: 823965. To enhance readability and language in this work, the author(s) employed ChatGPT-3.5 throughout the writing process. Following the use of this tool, the author(s) assumed full responsibility for the publication's content and reviewed and edited it as required.

Financial support

This research has been supported by the projects ET4DROUGHT (No. PID2021-127345OR-C31) and DIGISPAC (TED2021-131237B-C21) both funded by the Ministry of Science and Innovation (MICINN-AEI) of Spain.

References

Alarcón, J., Ortuño, M., Nicolás, E., Torres, R., Torrecillas, A.: Compensation heat-pulse measurements of sap flow for estimating transpiration in young lemon trees. Biol. Plant. 49, 527–532. https://doi.org/10.1007/s10535-005-0046-1, 2005.

Allen, R. Pereira, L., Raes, D. Smith, M.: Crops evapotranspiration: guidelines forcomputing crop water requirements. FAO Irrigation and Drainage Paper No. 56.FAO, Rome, Italy, 300, 1998

Allen, R., Tasumi, M., Morse, A., Trezza, R., Wright, J., Bastiaanssen, W., Kramber, W., Lorite, I., and Robison, C. W.: Satellite-Based Energy Balance for Mapping Evapotranspiration with Internalized Calibration (METRIC)—Applications, J. Irrig. Drain. Eng., 133, 395–406, https://doi.org/10.1061/(asce)0733-9437(2007)133:4(395), 2007.

Anderson, M., Norman, J., Diak, G., Kustas, W., Mecikalski, J.: A two-source time-integrated model for estimating surface fluxes using thermal infrared remote sensing. Remote Sens. Environ. 60, 195–216. https://doi.org/10.1016/S0034-4257(96)00215-5, 1997.

Anderson, M., Yang, Y., Xue, J., Knipper, K., Yang, Y., Gao, F., Hain, C., Kustas, W., Cawse-Nicholson, K., Hulley, G., Fisher, J., Alfieri, J., Meyers, T., Prueger, J., Baldocchi, D., and Rey-Sanchez, C.: Interoperability of ECOSTRESS and Landsat

for mapping evapotranspiration time series at sub-field scales, Remote Sens. Environ., 252, 112189, https://doi.org/10.1016/j.rse.2020.112189, 2021.

Basilio, R., Hook, S., Zoffoli, S. and Buongiorno, M.: Surface Biology and Geology (SBG) Thermal Infrared (TIR) Free - Flyer Concept.: 2022 IEEE Aerospace Conference (AERO), Big Sky, MT, USA, 01-09. 10.1109/AERO53065.2022.9843292, 2022.

Bastiaanssen, W., Pelgrum, H., Wang, J., Ma, Y., and Moreno, J. F.: A remote sensing surface energy balance algorithm for land (SEBAL).: Part 2: Validation, J. Hydrol., 212, 213–229, 1998.

Bellvert, J., Zarco-Tejada, P., Girona, J., and Fereres, E.: Mapping crop water stress index in a 'Pinot-noir' vineyard: Comparing ground measurements with thermal remote sensing imagery from an unmanned aerial vehicle, Precis. Agric., 15, 361–376, https://doi.org/10.1007/s11119-013-9334-5, 2014.

Brutsaert, W., and Sugita M.: Application of self-preservation in the diurnal evolution of the surface energy budget to determine daily evaporation, J Geophys Res, 97, 18377-18382, https://doi.org/10.1029/92JD00255, 1992.

Cammalleri, C., Anderson, M. C., and Kustas, W. P.: Upscaling of evapotranspiration fluxes from instantaneous to daytime scales for thermal remote sensing applications, Hydrol. Earth Syst. Sci., 18, 1885–1894, https://doi.org/10.5194/hess-18-1885-2014, 2014.

Campbell, G., Norman, J.: An introduction to environmental biophysics, second ed., Springer New York, NY., 286 pp., https://doi.org/10.1007/978-1-4612-1626-1, 1998.

Crago, R. and Brutsaert, W.: Daytime evaporation and the self-preservation of the evaporative fraction and the Bowen ratio, J. Hydrol., 178, 241–255, https://doi.org/10.1016/0022-1694(95)02803-x, 1996.

Castel, J. and Fereres, E.: Responses of Young Almond Trees to Two Drought Periods in the Field, J. Hortic. Sci., 57, 175–187, https://doi.org/10.1080/00221589.1982.11515038, 1982.

Chaves, M., Pereira, J. S., Maroco, J., Rodrigues, M., Ricardo, C., Osório, M., Carvalho, I., Faria, T., and Pinheiro, C.: How plants cope with water stress in the field. Photosynthesis and growth, Ann. Bot., 89, 907–916, https://doi.org/10.1093/aob/mcf105, 2002.

Colaizzi, P., Evett, S., Howell, T., and Tolk, J.: Comparison of five models to scale daily evapotranspiration from one-time-of-day measurements, 49, 1409–1418, 10.13031/2013.22056 ,2006.

Delogu, E., Boulet, G., Olioso, A., Coudert, B., Chirouze, J., Ceschia, E., Le Dantec, V., Marloie, O., Chehbouni, G., and Lagouarde, J. P.: Reconstruction of temporal variations of evapotranspiration using instantaneous estimates at the time of satellite overpass, Hydrol. Earth Syst. Sci., 16, 2995–3010, https://doi.org/10.5194/hess-16-2995-2012, 2012.

Drexler, J., Snyder, R., Spano, D., and Paw U.: A review of models and micrometeorological methods used to estimate wetland evapotranspiration, Hydrol. Process., 18, 2071–2101, https://doi.org/10.1002/hyp.1462, 2004.

Escalona, J., Flexas, J., and Medrano, H.: Stomatal and non-stomatal limitations of photosynthesis under water stress in field-grown grapevines, Aust. J. Plant Physiol., 26, 421–433, https://doi.org/10.1071/PP99019, 1999.

Espadafor, M., Orgaz, F., Testi, L., Lorite, I., Villalobos, F.: Transpiration of young almond trees in relation to intercepted radiation. Irrig. Sci. 33, 265–275. https://doi.org/10.1007/s00271-015-0464-6, 2015.

Evett, S. and Tolk, J.: Introduction: Can water use efficiency be modeled well enough to impact crop management?, Agron. J., 101, 423–425, https://doi.org/10.2134/agronj2009.0038xs, 2009.

Fernandez J., Palomo M., Díaz-Espejo A., Clothier B. , Green S., Girón I., Moreno F.: Heat-pulse measurements of sap flow in olives for automating irrigation: tests root flow and diagnostics of water stress. Agric Water Manag 51, 99–123. https:// doi. org/ 10. 1016/ S0378- 3774(01) 00119-6, 2001.

Forster, M.: How Reliable Are Heat Pulse Velocity Methods for Estimating Tree Transpiration? Forests 8, 350. https://doi.org/10.3390/f8090350, 2017.

Gao, R., Torres-Rua, A., Aboutalebi, M., White, W., Anderson, M., Kustas, W., Agam, N., Alsina, M., Alfieri, J., Hipps, L., Dokoozlian, N., Nieto, H., Gao, F., McKee, L., Prueger, J., Sanchez, L., Mcelrone, A., Bambach-Ortiz, N., Coopmans, C., and Gowing, I.: LAI estimation across California vineyards using sUAS multi-seasonal multi-spectral, thermal, and elevation information and machine learning, Irrig. Sci., https://doi.org/10.1007/s00271-022-00776-0, 2022.

Gao, R., Torres-Rua, A., Nieto, H., Zahn, E., Hipps, L., Kustas, W., Alsina, M., Bambach, N., Castro, S., Prueger, J., Alfieri, J., Mckee, L., White, W., Gao, F., Mcelrone, A., Anderson, M., Knipper, K., and Coopmans, C.: ET Partitioning Assessment Using the TSEB Model and sUAS Information across California Central Valley Vineyards, https://doi.org/10.3390/rs15030756, 2023.

Gentine, P., Entekhabi, D., Chehbouni, A., Boulet, G., and Duchemin, B.: Analysis of evaporative fraction diurnal behaviour, Agric. For. Meteorol., 143, 13–29, https://doi.org/10.1016/j.agrformet.2006.11.002, 2007.

Goldhamer, D. A. and Fereres, E.: Establishing an almond water production function for California using long-term yield response to variable irrigation, Irrig. Sci., 35, 169–179, https://doi.org/10.1007/s00271-016-0528-2, 2017.

Gómez-Candón, D., Bellvert, J., and Royo, C.: Performance of the Two-Source Energy Balance (TSEB) Model as a Tool for Monitoring the Response of Durum Wheat to Drought by High-Throughput Field Phenotyping, Front. Plant Sci., 12, https://doi.org/10.3389/fpls.2021.658357, 2021.

Hoedjes, J., Chehbouni, A., Jacob, F., Ezzahar, J., and Boulet, G.: Deriving daily evapotranspiration from remotely sensed instantaneous evaporative fraction over olive orchard in semi-arid Morocco, J. Hydrol., 354, 53–64, https://doi.org/10.1016/j.jhydrol.2008.02.016, 2008.

Iglesias, I. and Echeverria, G.: Scientia Horticulturae Current situation , trends and challenges for efficient and sustainable peach production, Sci. Hortic., 296, 110899, https://doi.org/10.1016/j.scienta.2022.110899, 2022.

Jackson, R., Hatfield, J., Reginato, R., Idso, S., and Pinter, P.: Estimation of daily evapotranspiration from one time-of-day measurements, Agric. Water Manag., 7, 351–362, https://doi.org/10.1016/0378-3774(83)90095-1, 1983.

Jiang, L., Zhang, B., Han, S., Chen, H., and Wei, Z.: Upscaling evapotranspiration from the instantaneous to the daily time scale: Assessing six methods including an optimized coefficient based on worldwide eddy covariance flux network, J. Hydrol., 596, 126135, https://doi.org/10.1016/j.jhydrol.2021.126135, 2021.

Jofre-Čekalović, C., Nieto, H., Girona, J., Pamies-Sans, M., and Bellvert, J.: Accounting for Almond Crop Water Use under Different Irrigation Regimes with a Two-Source Energy Balance Model and Copernicus-Based Inputs, Remote Sens., 14, 2106, https://doi.org/10.3390/rs14092106, 2022.

Kalma, J., McVicar, T., and McCabe, M.: Estimating land surface evaporation: A review of methods using remotely sensed surface temperature data, Surv. Geophys., 29, 421–469, https://doi.org/10.1007/s10712-008-9037-z, 2008.

Knipper, K., Anderson, M., Bambach, N., Kustas, W., Gao, F., Zahn, E., Hain, C., McElrone, A., Belfiore, O., Castro, S., Alsina, M., and Saa, S.: Evaluation of Partitioned Evaporation and Transpiration Estimates within the DisALEXI Modeling Framework over Irrigated Crops in California, Remote Sens., 15, https://doi.org/10.3390/rs15010068, 2023.

Koetz, B., Bastiaanssen, W., Berger, M., Defourney, P., Bello, U. Del, Drusch, M., Drinkwater, M., Duca, R., Fernandez, V., Ghent, D., Guzinski, R., Hoogeveen, J., Hook, S., Lagouarde, J. P., Lemoine, G., Manolis, I., Martimort, P., Masek, J., Massart, M., Notarnicola, C., Sobrino, J., and Udelhoven, T.: High spatio-temporal resolution land surface temperature mission - A Copernicus candidate mission in support of agricultural monitoring, Int. Geosci. Remote Sens. Symp., 2018-July, 8160–8162, https://doi.org/10.1109/IGARSS.2018.8517433, 2018.

Kustas, W. and Anderson, M.: Advances in thermal infrared remote sensing for land surface modeling, Agric. For. Meteorol., 149, 2071–2081, https://doi.org/10.1016/j.agrformet.2009.05.016, 2009.

Kustas, W., Alfieri, J., Nieto, H., Wilson, T., Gao, F., Anderson, M.: Utility of the two-source energy balance (TSEB) model in vine and interrow flux partitioning over the growing season. Irrig. Sci. 37, 375–388. https://doi.org/10.1007/s00271-018-0586-8, 2019.

Kustas, W. and Norman, J.: Evaluation of soil and vegetation heat flux predictions using a simple two-source model with radiometric temperatures for partial canopy cover, Agric. For. Meteorol., 94, 13–29, https://doi.org/10.1016/S0168-1923(99)00005-2, 1999.

Kustas, W., Nieto, H., Garcia-Tejera, O., Bambach, N., McElrone, A., Gao, F., Alfieri, J., Hipps, L., Prueger, J., Torres-Rua, A., Anderson, M., Knipper, K., Alsina, M., McKee, L., Zahn, E., Bou-Zeid, E., Dokoozlian, N.: Impact of advection on two-source energy balance (TSEB) canopy transpiration parameterization for vineyards in the California Central Valley. Irrig. Sci. 40, 575–591. https://doi.org/10.1007/s00271-022-00778-y, 2022.

Lagouarde, J., Bhattacharya, B., Crébassol, P., Gamet, P., Babu, S., Boulet, G., Briottet, X., Buddhiraju, K., Cherchali, S., Dadou, I., Dedieu, G., Gouhier, M., Hagolle, O., Irvine, M., Jacob, F., Kumar, A., Kumar, K., Laignel, B., Mallick, K., Murthy, C., Olioso, A., Ottlé, C., Pandya, M., Raju, P., Roujean, J., Sekhar, M., Shukla, M., Singh, S., Sobrino, J., and Ramakrishnan, R.: The Indian-French Trishna mission: Earth observation in the thermal infrared with high spatio-temporal resolution, Int. Geosci. Remote Sens. Symp., 2018-July, 4078–4081, https://doi.org/10.1109/IGARSS.2018.8518720, 2018.

Lhomme, J. and Elguero, E.: Examination of evaporative fraction diurnal behaviour using a soil-vegetation model coupled with a mixed-layer model, https://doi.org/10.5194/hess-3-259-1999, 1999.

López-Bernal, Á., Alcántara, E., Testi, L., and Villalobos, F.: Spatial sap flow and xylem anatomical characteristics in olive trees under different irrigation regimes, Tree Physiol., 30, 1536–1544, https://doi.org/10.1093/treephys/tpq095, 2010.

López-López, M., Espadador, M., Testi, L., Lorite, I., Orgaz, F., and Fereres, E.: Water use of irrigated almond trees when subjected to water deficits, Agric. Water Manag., 195, 84–93, https://doi.org/10.1016/j.agwat.2017.10.001, 2018.

McCutchan, H., Shackel, K.: Stem-water potential as a sensitive indicator of water stress in prune trees (Prunus domestica L. cv. French). J Am Soc Hortic Sci. 117, 607–611, 1992.

Mwangi, S., Boulet, G., and Olioso, A.: Assessment of an extended SPARSE model for estimating evapotranspiration from directional thermal infrared data, Agric. For. Meteorol., 317, 108882, https://doi.org/10.1016/j.agrformet.2022.108882, 2022.

Mwangi, S., Boulet, G., Le Page, M., Gastellu-Etchegorry, J., Bellvert, J., Lemaire, B., Fanise, P., Roujean, J., and Olioso, A.: Observation and Assessment of Model Retrievals of Surface Exchange Components over a Row Canopy Using Directional Thermal Data, IEEE J. Sel. Top. Appl. Earth Obs. Remote Sens., 16, 7343–7356, https://doi.org/10.1109/JSTARS.2023.3297709, 2023.

Nassar, A., Torres-Rua, A., Kustas, W., Nieto, H., McKee, M., Hipps, L., Stevens, D., Alfieri, J., Prueger, J., Alsina, M., McKee, L., Coopmans, C., Sanchez, L., and Dokoozlian, N.: Influence of model grid size on the estimation of surface fluxes using the two source energy balance model and sUAS imagery in vineyards, Remote Sens., 12, https://doi.org/10.3390/rs12030342, 2020.

Nassar, A., Torres-Rua, A., Kustas, W., Alfieri, J., Hipps, L., Prueger, J., Nieto, H., Alsina, M., White, W., McKee, L., Coopmans, C., Sanchez, L., and Dokoozlian, N.: Assessing daily evapotranspiration methodologies from one-time-of-day Suas and EC information in the GRAPEX project, Remote Sens., 13, https://doi.org/10.3390/rs13152887, 2021.

Nieto, H., Kustas, W., Torres-Rua, A., Alfieri, J., Gao, F., Anderson, M., White, W., Song, L., Alsina, M., Prueger, J., McKee, M., Elarab, M., and McKee, L.: Evaluation of TSEB turbulent fluxes using different methods for the retrieval of soil and canopy component temperatures from UAV thermal and multispectral imagery, Irrig. Sci., 37, 389–406, https://doi.org/10.1007/s00271-018-0585-9, 2019.

Norman, J., Kustas, W., and Humes, K.: Source approach for estimating soil and vegetation energy fluxes in observations of directional radiometric surface temperature, Agric. For. Meteorol., 77, 263–293, https://doi.org/10.1016/0168-1923(95)02265-Y, 1995.

Olivo, N., Girona, J., and Marsal, J.: Seasonal sensitivity of stem water potential to vapour pressure deficit in grapevine, Irrig. Sci., 27, 175–182, https://doi.org/10.1007/s00271-008-0134-z, 2009.

Overgaard, J., Rosbjerg, D., and Butts, M.: Land-surface modelling in hydrological perspective - A review, Biogeosciences, 3, 229–241, https://doi.org/10.5194/bg-3-229-2006, 2006.

Parry, C., Nieto, H., Guillevic, P., Agam, N., Kustas, W., Alfieri, J., McKee, L., and McElrone, A.: An intercomparison of radiation partitioning models in vineyard canopies, Irrig. Sci., 37, 239–252, https://doi.org/10.1007/s00271-019-00621-x, 2019.

Peddinti, S. and Kisekka, I.: Estimation of turbulent fluxes over almond orchards using high-resolution aerial imagery with one and two-source energy balance models, Agric. Water Manag., 269, 107671, https://doi.org/10.1016/j.agwat.2022.107671, 2022.

Poni, S., Bernizzoni, F., Civardi, S., Gatti, M., Porro, D., and Camin, F.: Performance and water-use efficiency (single-leaf vs. whole-canopy) of well-watered and half-stressed split-root Lambrusco grapevines grown in Po Valley (Italy), Agric. Ecosyst. Environ., 129, 97–106, https://doi.org/10.1016/j.agee.2008.07.009, 2009.

Qi, J., Chehbouni, A., Huete, A., Kerr, Y., and Sorooshian, S.: A modified soil adjusted vegetation index, Remote Sens. Environ., 48, 119–126, https://doi.org/10.1016/0034-4257(94)90134-1, 1994.

Quintanilla-Albornoz, M., Miarnau, X., Pelechá, A., Casadesús, J., García-Tejera, O., and Bellvert, J.: Evaluation of transpiration in different almond production systems with two-source energy balance models from UAV thermal and multispectral imagery, Irrig. Sci., https://doi.org/10.1007/s00271-023-00888-1, 2023.

Romero, P. and Botía, P.: Daily and seasonal patterns of leaf water relations and gas exchange of regulated deficit-irrigated almond trees under semiarid conditions, Environ. Exp. Bot., 56, 158–173, https://doi.org/10.1016/j.envexpbot.2005.01.012, 2006.

Sánchez, J, Simón L., González-Piqueras. J., and Montoya F.: Monitoring Crop Evapotranspiration and Transpiration / Evaporation Partitioning in a Drip-Irrigated, Water (Switzerland), https:// doi.org/10.3390/w13152073, 2021.

Shuttleworth, W., Gurney, R., Hsu, A., and Ormsby, J.: FIFE: the variation in energy partition at surface flux sites, Remote Sens. Large-Scale Glob. Porc. (IAHS Publ.), 186, 67–74, 1989.

Shuttleworth, W. and Wallace, J.: Evaporation from sparse crops-an energy combination theory, Q. J. R. Meteorol. Soc., 111, 839–855, https://doi.org/10.1002/qj.49711146510, 1985.

Smith, D., Allen, S.: Measurement of sap flow in plant stems. J. Exp. Bot. 47, 1833–1844. https://doi.org/10.1093/jxb/47.12.1833, 1996

Tian, T. and Schreiner, R.: Appropriate time to measure leaf and stem water potential in north-south oriented, vertically shoot-positioned vineyards, Am. J. Enol. Vitic., 72, 64–72, https://doi.org/10.5344/ajev.2020.20020, 2021.

Timmermans, W., Kustas, W., Anderson, M., and French, A.: An intercomparison of the Surface Energy Balance Algorithm for Land (SEBAL) and the Two-Source Energy Balance (TSEB) modeling schemes, Remote Sens. Environ., 108, 369–384, https://doi.org/10.1016/j.rse.2006.11.028, 2007.

Trezza, R.: Evapotranspiration using a satellite-based surface energy balance with standardized ground control, Doctoral dissertation, Utah State University, 2002.

Tuzet, A., Perrier A., and Leuning R.: A coupled model of stomatal conductance, photosynthesis and transpiration. Plant, Cell & Environment, 26, 1097–1116, https://doi.org/10.1046/j.1365-3040.2003.01035.x, 2003.

Van Niel. T., McVicar T., Roderick M., Van Dijk A., Renzullo L., Van Gorsel E.: Correcting for systematic error in satellite-derived latent heat flux due to assumptions in temporal scaling: Assessment from flux tower observations. J Hydrol., 409:140–148. https://doi.org/10.1016/j.jhydrol.2011.08.011, 2011.

Van Niel, T., McVicar, T., Roderick, M., Van Dijk, A., Beringer, J., Hutley, L., and Van Gorsel, E.: Upscaling latent heat flux for thermal remote sensing studies: Comparison of alternative approaches and correction of bias, J. Hydrol., 468–469, 35–46, https://doi.org/10.1016/j.jhydrol.2012.08.005, 2012.

Villalobos, F., Testi, L., and Moreno-Perez, M.: Evaporation and canopy conductance of citrus orchards, Agric. Water Manag., 96, 565–573, https://doi.org/10.1016/j.agwat.2008.09.016, 2009.

Xu, T., Guo, Z., Liu, S., He, X., Meng, Y., Xu, Z., Xia, Y., Xiao, J., Zhang, Y., Ma, Y., and Song, L.: Evaluating Different Machine Learning Methods for Upscaling Evapotranspiration from Flux Towers to the Regional Scale, J. Geophys. Res. Atmos., 123, 8674–8690, https://doi.org/10.1029/2018JD028447, 2018.

Zhang, J., Guan, K., Peng, B., Jiang, C., Zhou, W., Yang, Y., Pan, M., Franz, T., Heeren, D., Rudnick, D., Abimbola, O., Kimm, H., Caylor, K., Good, S., Khanna, M., Gates, J., and Cai, Y.: Challenges and opportunities in precision irrigation decision-support systems for center pivots, Environ. Res. Lett., 16, https://doi.org/10.1088/1748-9326/abe436, 2021.

Zhang, L. and Lemeur, R.: Evaluation of daily evapotranspiration estimates from instantaneous measurements, Agric. For. Meteorol., 74, 139–154, https://doi.org/10.1016/0168-1923(94)02181-I, 1995.